Available online at www.sciencedirect.com

SCIENCE DIRECT®

Tectonophysics 391 (2004) 203–237

TECTONOPHYSICS

www.elsevier.com/locate/tecto

Kinematic consistency between the Dead Sea Fault Zone and the Neogene and Quaternary left-lateral faulting in SE Turkey

Rob Westaway

16 Neville Square, Durham DH1 3PY, United Kingdom

Accepted 3 June 2004
Available online 8 October 2004

Abstract

A revised quantitative kinematic model has been determined for the Dead Sea Fault Zone (DSFZ) and the left-lateral fault zones in SE Turkey. The relative motions of the African and Arabian plates across the DSFZ are represented by relative rotation about 31.1°N 26.7°E at 0.40±0.02° Ma^{-1}. The northern DSFZ, in Syria and southern Turkey, is interpreted for the first time as a series of transpressional stepovers, along which the left-lateral slip rate is substantially less than the rate of relative plate motion, because this slip is oblique to the plate motion. The slip rate on the East Anatolian Fault Zone (EAFZ) is estimated as ~8 mm a^{-1}. Restoring its observed slip thus requires its age to be ~4 Ma. The previous phase of deformation, which involved slip on the Malatya–Ovacık Fault Zone (MOFZ) before the EAFZ came into being, is thus dated to ~7–4 Ma, suggesting initiation of the North Anatolian Fault Zone (NAFZ) at ~7 Ma, not ~5 Ma as previously thought. The total left-lateral slip on the northern DSFZ in southernmost Turkey is estimated as at least ~65 km, partitioned with ~45 km on the Amanos Fault, ~10 km on the East Hatay Fault, and a further ~10 km on the Kırkpınar Fault farther east. Much of this slip is inferred to have occurred during the Miocene, before the modern geometry of this plate boundary zone developed. When it first formed, the AF–AR plate boundary was relatively complex—it initially reactivated preexisting structures in the Palmyra foldbelt in Syria and in the Gaziantep region of southern Turkey, which were significantly misaligned relative to the plate motion, requiring major components of shortening as well as left-lateral slip. The transition, from this initial rather diffuse geometry to the present localised geometry of the DSFZ across western Syria, occurred within the Miocene. The predicted rate of relative motion between the stable interiors of the Turkish and African plates in the vicinity of their common boundary onshore of İskenderun Gulf in southern Turkey is estimated as westward at ~9 mm a^{-1}. However, this "promontory" of the African plate is itself moving westward relative to the stable interior of this plate at ~7–8 mm a^{-1}. The rate of localised left-lateral slip on the onshore part of this boundary, the NE-trending Yakapınar–Göksun Fault, is thus estimated as only ~2 mm a^{-1}. This locality can also be regarded as within the distributed boundary zone between the Turkish and Arabian plates. The estimated relative motion between these plates is at ~8.7 mm a^{-1} towards the SSW, partitioned between localised left-lateral slip at ~2 mm a^{-1} on the Yakapınar–Göksun Fault, and at least ~1 mm a^{-1} on the Amanos Fault, and ~2.5 mm a^{-1} on East Hatay Fault, with at most distributed left-lateral simple shear at ~3.2 mm a^{-1} across the Amanos Mountains in between. However, the combined slip on left-lateral faults east of the Amanos Mountains may be as high as ~6 mm a^{-1}, with slip at ~1.7 mm a^{-1} on the Amanos Fault and at ~4.3 mm a^{-1} on the East Hatay Fault and any active faults farther east. This requires no more than ~0.7 mm a^{-1} of

E-mail address: r.w.c.westaway@ncl.ac.uk.

doi:10.1016/j.tecto.2004.07.014

distributed simple shear across the Amanos Mountains, raising the possibility that this component of deformation may in fact be zero, this small nonzero estimate possibly indicating a closure error arising from minor errors in predicted values of other relative motion vectors. It is proposed that this boundary between the Turkish and African plates first developed at the same time as the MOFZ and NAFZ, but its original geometry involving left-lateral slip on the Karataş–Osmaniye Fault has since become locked by the presence of relatively strong ophiolitic crust within this fault zone. This quantitative kinematic model demonstrates, for the first time, how it is possible for the left-lateral faulting accommodating the NNW–SSE relative motion between the Arabian and African plates in NW Syria to "dovetail" into the left-lateral faulting accommodating the WSW–ENE relative motion between the Turkish and Arabian plates in SE Turkey.

Keywords: Turkey; Syria; Israel; Lebanon; East Anatolian fault Zone; Dead Sea Fault Zone; Plate kinematics; Quaternary; Pliocene

1. Introduction

Active crustal deformation in and around Turkey reflects the interaction between the Eurasian, African, Arabian, and Turkish plates (Fig. 1). The Turkish plate (TR) is bounded to the north by the right-lateral North Anatolian Fault Zone (NAFZ), which separates it from Eurasia (EU), and to the south and west by the

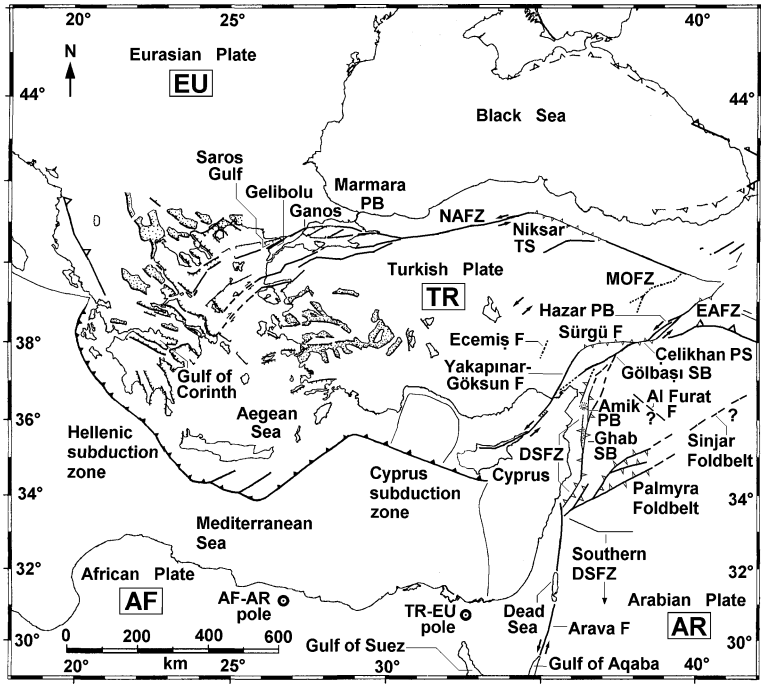

Fig. 1. Map of the present study region. Fault geometry is summarised from Westaway and Arger (1996, 2001), McClusky et al. (2000), Westaway (2002b), and this study. DSFZ, EAFZ, NAFZ, and MOFZ indicate the Dead Sea Fault Zone, East Anatolian Fault Zone, North Anatolian Fault Zone, and Malatya–Ovacık Fault Zone. The Al Furat Fault and Sinjar fold belt, possible continuations of the active crustal deformation in the Palmyra fold belt involving NW–SE left-lateral slip and/or NW–SE shortening, are summarised from Lovelock (1984). Structures are classified using the following abbreviations: fault (F), pull-apart basin (PB), transpressional stepover (PS), splay basin (SB), and transtensional stepover (TS). Positions of preferred Euler poles, for the relative motions of the African and Arabian plates (AF–AR; from Klinger et al., 2000), and the Turkish and European plates (TR–EU; from McClusky et al., 2000), are labelled. Note that the TR-EU pole is concentric to almost the whole NAFZ, consistent with right-lateral transform faulting. However, the AF-AR pole is only concentric to the southern DSFZ—it requires left-lateral transpression, not transform faulting, farther north.

active plate margin formed by the Hellenic and Cyprus trenches, where the African plate (AF) is subducting northward. The NAFZ dies out southwestward into the distributed crustal extension within the Aegean region, overlying the Hellenic subduction zone. The eastern boundary of the Turkish plate is a complex left-lateral strike-slip fault zone, adjoining both the African and Arabian (AR) plates. The TR–AR plate boundary follows the left-lateral East Anatolian Fault Zone (EAFZ), which splays southwestward in SE Turkey into the TR–AF and AF–AR plate boundaries, the latter being known as the Dead Sea Fault Zone (DSFZ).

Westaway (1994) published the first internally consistent quantitative kinematic model for this region, which constrained the senses and rates of slip on each of these fault zones individually using local evidence and then demonstrated the overall kinematic consistency of the scheme. This approach superseded other investigations, such as Jackson and McKenzie (1988), who determined slip rates on individual fault zones in this region without regard for their overall consistency, or Dewey et al. (1986) and Karig and Kozlu (1990) who determined qualitative kinematic models for the senses (but not the rates) of crustal deformation. The aim of this study is to update this model to take account of the subsequent development of quantitative theory for investigating strike-slip faulting oriented oblique to the relative motions of the adjoining plates (Westaway, 1995) and to incorporate new information from GPS investigations in Turkey (e.g., McClusky et al., 2000) and from recent detailed field observations—notably from within Syria. To keep this study focussed, it will only concentrate on new data that contributes usefully to improving constraint on the regional kinematics. For instance, some recent studies have proposed that the Ecemiş Fault in central–southern Turkey (Fig. 1) is slipping so fast that it should be considered on a par with the NAFZ and EAFZ—a view that can be emphatically contradicted (e.g., Westaway, 1990, 2002a), as radiocarbon dating (Çetin, 2000) constrains its slip rate to ~0.03 mm a^{-1}. However, no attempt is made here to review every such contribution to the literature.

This study will, first, discuss the available evidence from each major zone of strike-slip faulting in turn. It will then demonstrate the extent of the consistency between this model and the available evidence, before discussing possible adjustments that can improve this consistency further.

2. The Dead Sea Fault Zone

The DSFZ (Fig. 1) consists of a N–S trending southern segment, which bounds Israel and Jordan and links southward through the Gulf of Aqaba and Tiran Strait to the oceanic spreading centre in the Red Sea, a central segment oriented N30°E across Lebanon, and a northern segment that trends N–S across Syria but bends towards the NNE and splays into en echelon fault strands (Fig. 2) in southern Turkey. The total slip on the DSFZ has been estimated as ~105 km in the south (e.g., Freund et al., 1970; Garfunkel, 1981; Quennell, 1984) and ~70–80 km in the north (e.g., Freund et al., 1970; Dewey et al., 1986). The ~105-km estimate in the south is based on matching many independent features across the southern DSFZ. In contrast, the ~70- to 80-km estimate in the Turkey–Syria border region is based on projecting the southern outline of outcrops of the Hatay/Baer-Bassit ophiolite on the African side (K–L in Fig. 3) into the line of the DSFZ in the Orontes valley (to the north of I in Fig. 3), and matching it against the southern margin of the ophiolite farther north on the Arabian side, around locality C (Fig. 3). However, as Yurtmen et al. (2002) noted, this estimate excludes the slip on the Afrin Fault that runs east of the Hatay ophiolite (Figs. 2 and 3). That is, it only covers the Amanos and East Hatay faults. In addition, although this southern margin of the ophiolite directly abuts the East Hatay Fault to the east, south of Tahtaköprü (C in Fig. 3), its supposed counterpart—west of the DSFZ SE of Antakya (K–L in Fig. 3)—is more than ~10 km from the DSFZ (Fig. 3), sufficiently distant that associating it with any specific outcrop on the opposite side seems arbitrary. The southernmost points where ophiolite crops out directly adjacent to the western margin of the DSFZ are around the SW corner of the Amik Basin north and northeast of Antakya (e.g., G or H in Fig. 3). The southernmost point where ophiolite crops out immediately east of the Amanos Fault was identified by Yurtmen et al. (2002) as between the villages of Bektaşlı and Dokuzlar (see also Atan, 1969; Figs. 2 and 3), some ~45–50 km farther north (F in Fig. 3). Yurtmen et al. (2002) suggested that the East Hatay

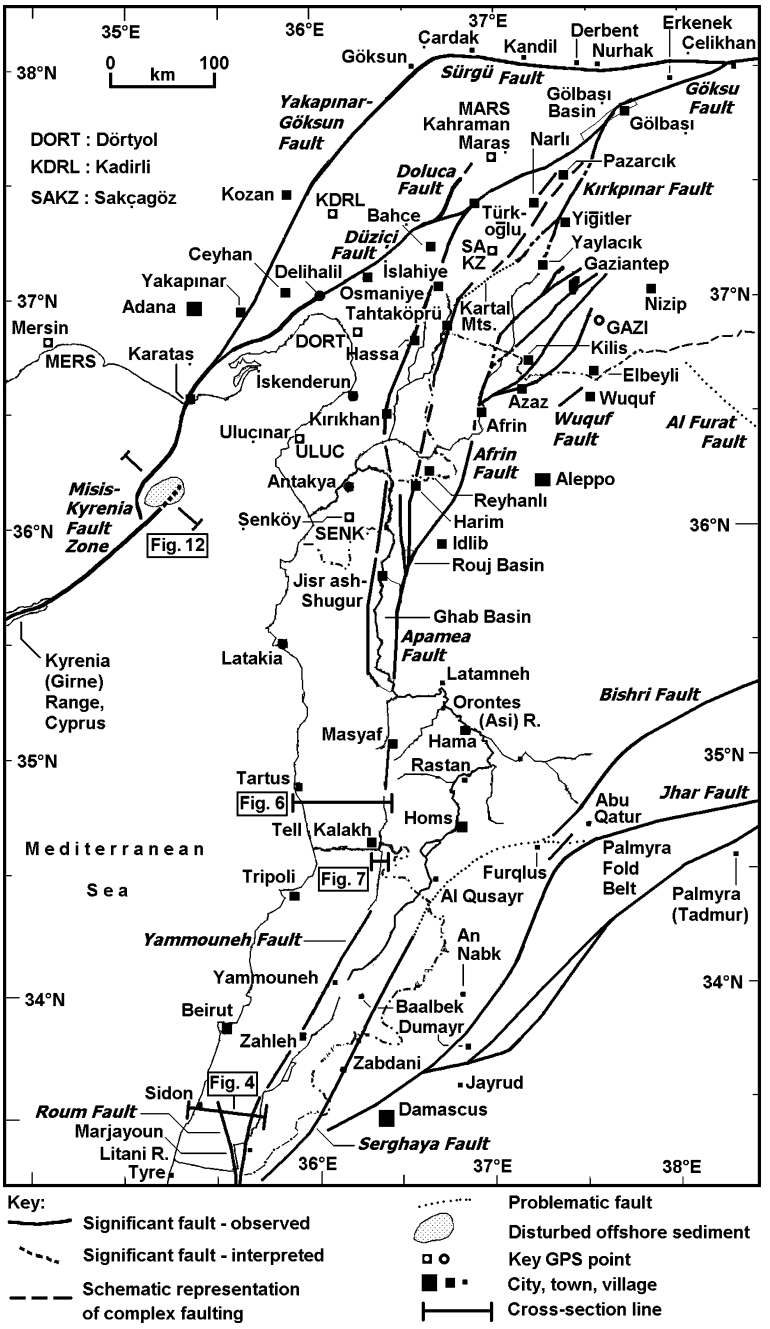

Fig. 2. Map of significant fault segments of the TR–AR and TR–AF plate boundaries linking southeast Turkey, Lebanon, and Cyprus, in relation to GPS points, from McClusky et al. (2000). Faults in Lebanon and southern Syria are from Ponikarov et al. (1966) and Walley (1998). Those in northern Syria are from Ponikarov et al. (1966) and the analysis in this study. Faults in and offshore of southern Turkey are from Aksu et al. (1992), Westaway and Arger (1996), Terlemez et al. (1997), Coşkun and Coşkun (2000), Yurtmen and Westaway (2001b), Yurtmen et al. (2002), and the analysis in this study. The three "problematical faults" shown are the NE continuation of the Serghaya Fault across the Homs area of Syria, from Walley (1998), which—if it exists— appears to have not been active since at least the Early Pliocene (see Fig. 5 and its caption), the NW end of the Al Furat Fault (Lovelock, 1984), and the "Kartal Fault" of Westaway and Arger (1996) in southern Turkey, which is a misinterpretation.

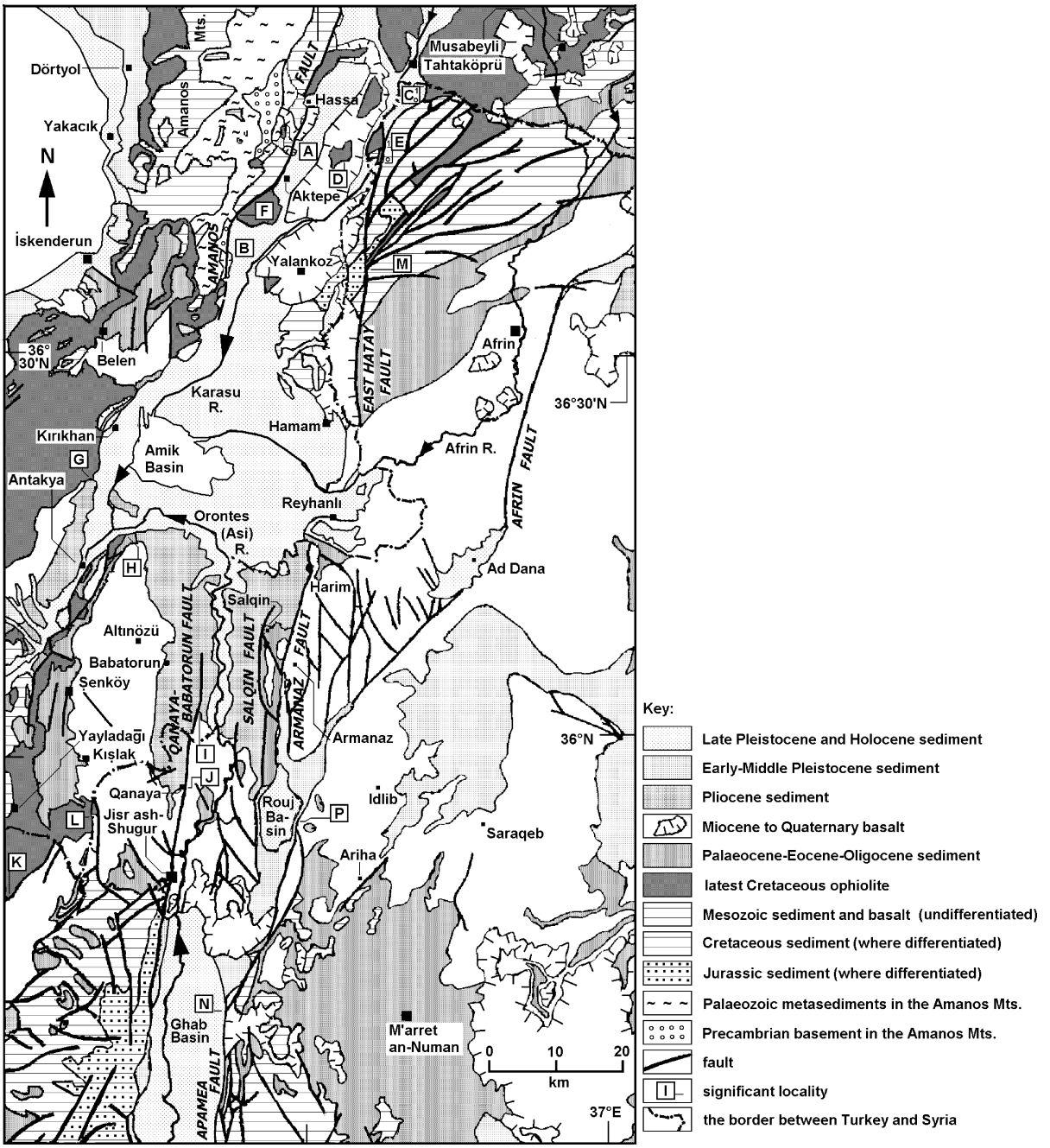

Fig. 3. Maps of possible piercing points across the northern DSFZ. Adapted from Tolun and Erentöz (1962) and Ponikarov et al. (1966). M indicates the southern margin of an outcrop of Late Jurassic limestone that appears to be offset left laterally by ~3 km across the East Hatay Fault. The other piercing points are explained in the text. Some detail in Syria should be regarded as tentative, as some details conflict between the Ponikarov et al. (1966) map and either figures in the Ponikarov et al. (1967) guide or later references. See text for discussion.

Fault could have slipped by ~15 km based on the N–S separation of the southernmost serpentinite outcrops on either side of it (D-C1 in Fig. 3). Better estimates can instead be obtained from the N–S offset measured between locality D, just inside Syria on the Africa side of the East Hatay Fault, and locality C on the Arabian side. The southern margin of serpentinite is offset ~10 km (E1–C1 in Fig. 3), as is the southern margin of radiolarian chert located ~3 km farther south (Eo–Co in Fig. 3). The combined slip on the Amanos and East Hatay Fault may thus be as little as ~55 km. The component of slip on the Afrin Fault farther east remains unknown.

To check this ~55-km estimate, investigations have been made of the structure and lateral facies variations in the Mesozoic and Tertiary rocks exposed in the Amanos Mountains between Kırıkhan and Hassa and in the uplands to the west of Gaziantep (e.g., Atan, 1969; Terlemez et al., 1997). Although some broadly equivalent features have been identified, how to project them onto the line of the fault zone to establish them as piercing points remains problematic. I thus do not discuss this evidence further at this stage. It is nonetheless evident that the northern DSFZ could readily have slipped by many tens of kilometres, but probably tens of kilometres *less* than the southern DSFZ has slipped.

The age of the DSFZ has been estimated in many studies as ~15–19 Ma (e.g., Garfunkel, 1981; Ginat et al., 1998). The upper age bound of 19 Ma exists because basaltic dykes of this age exposed in Sinai are offset by the full ~105-km distance from their counterparts east of the DSFZ in Jordan (e.g., Eyal et al., 1981; Steinitz et al., 1981). The age of the central and northern DSFZ has instead proved controversial. Some studies (e.g., Freund et al., 1970; Dewey et al., 1986; Westaway, 1994; Yurtmen et al., 2002) have assumed that it formed at the same time as the southern DSFZ and has continued to slip to the present day. Others (e.g., Girdler, 1990; Butler et al., 1997, 1998; Butler and Spencer, 1999) have suggested that it formed at the same time as the southern DSFZ but (notwithstanding its obvious historical seismicity) somehow ceased to be active sometime around the Late Miocene when slip migrated onto another (hypothetical) fault zone located offshore to the west. Others (e.g., Brew et al., 2001) have suggested in contrast that the northern DSFZ did not become active until the Early Pliocene. Simple fieldwork in western Syria and analysis of the kinematics (see below) allow one to distinguish between these contradictory hypotheses, in favour of the first one.

The Westaway (1994) kinematic model assumed (1) that both N- to S-trending DSFZ segments are transform faults and (2) their slip rate can be estimated by dividing the ~105-km total slip by the ~15-Ma estimated age to obtain ~7 mm a^{-1}. Ben-Menahem (1981) and Westaway (1994) also obtained slip rate estimates of ~6 mm a^{-1} using seismic moment summation for historical earthquakes. The central DSFZ segment through the mountains of Lebanon is of course a transpressive stepover with more complex kinematics (e.g., Westaway, 1995). The major revision proposed in this study is that the northern DSFZ is reinterpreted as another transpressive stepover (at a more acute angle than the Lebanon stepover) and not a transform fault zone. The proposed model adopts the DSFZ Euler pole from Klinger et al. (2000), at 31.1°N 26.7°E, which is well fitted using a range of Late Quaternary kinematic indicators. However, rather than adopting their relative rotation rate of 0.396° Ma^{-1} it considers a range of values, a lower bound of 0.385° Ma^{-1} and an upper bound of 0.42° Ma^{-1}, which lead to a nominal estimate of $0.40\pm0.02°$ Ma^{-1}. With this new lower bound to the Euler vector, rates of AR–AF relative motion increase northward, away from the pole, from ~5.5 mm a^{-1} in Israel to ~7.8 mm a^{-1} in southern Turkey. However, taking account of the inferred transpressive geometry of the northern DSFZ, the highest predicted rate of left-lateral slip is ~6.1 mm a^{-1} in Syria. This exceeds the ~4.5 mm a^{-1} predicted left-lateral slip rate in southern Turkey, where the DSFZ is severely misaligned with respect to the relative plate motion. This set of values and the corresponding estimates for the upper bound to the relative rotation rate are shown to be roughly consistent with slip rates on the DSFZ recently deduced in Syria by trenching (Meghraoui et al., 2001, 2003; Meghraoui, 2002) and in the Karasu Valley of southern Turkey from offset Quaternary basalt flows and other evidence (Yurtmen et al., 2002). They are also consistent with recent geodetic solutions for the kinematics of the EAFZ and for the strike-slip faulting in the extreme south of Turkey (e.g. McClusky et al., 2000), as well as field-based solutions for the TR–AF plate boundary (Yurtmen and

Westaway, 2001a). In contrast, these predictions exceed the rates of ~4 mm a^{-1} or less estimated in several recent studies of the southern DSFZ (e.g., Ellembum et al., 1998; Ginat et al., 1998; Zhang, 1998; Klinger et al., 2000). It is thus presumed that these studies missed part of the overall slip rate due to the presence of multiple en-echelon fault strands in their study localities.

2.1. The Lebanon stepover and Palmyra Foldbelt

Within Lebanon, the DSFZ typically trends N30°E, its main strand—delineating the western margin of the Bekaa Valley and the eastern flank of the Lebanon mountain range—being known as the Yammouneh Fault (e.g., Walley, 1998). Other significant left-lateral fault segments are also present, notably the Serghaya Fault (e.g., Gomez et al., 2001a,b), which forms the eastern margin of the Bekaa Valley and the western flank of the Anti-Lebanon mountains, and the Roum Fault. The Roum Fault splays from the Yammouneh Fault at the southern end of the Lebanon stepover (Fig. 2), with a trend of N12°W (Griffiths et al., 2000) that is subparallel to the N14°W tangential direction to the preferred AF–AR Euler pole. The surroundings to these faults are pervasively fractured by minor faulting, and folded (e.g., Westaway, 1995; Walley, 1998; Griffiths et al., 2000) (Fig. 4). They are also tilted away from the Yammouneh Fault on both sides. That is, in the escarpment adjacent to this fault, Jurassic and Cretaceous rocks are exposed, the Tertiary sequence formerly covering them having been eroded, this tilting dying out over distances of up to ~20 km, where the Tertiary sequence is preserved and exposed (e.g., Walley, 1998) (Fig. 4).

Attempts at explaining the kinematics of this structure in terms of rigid blocks bounded by transform faults oriented oblique to the plate motion (e.g., Walley, 1988) clearly do not work (e.g., Westaway, 1995). This led to the suggestion (Westaway, 1995) that the left-lateral faults within this structure are not transform faults—they are instead bounding blocks that are themselves deforming internally, this deformation including components of distributed left-lateral simple shear and/or distributed shortening. Westaway (1995) determined the velocity gradient tensor and deformation gradient tensor describing this situation, in which an internal strike-slip fault, within the structure, is slipping at a rate U and oriented at an angle θ to adjoining transform faults that are themselves oriented parallel to the motion of the adjoining plates and slipping at rate V. In addition to

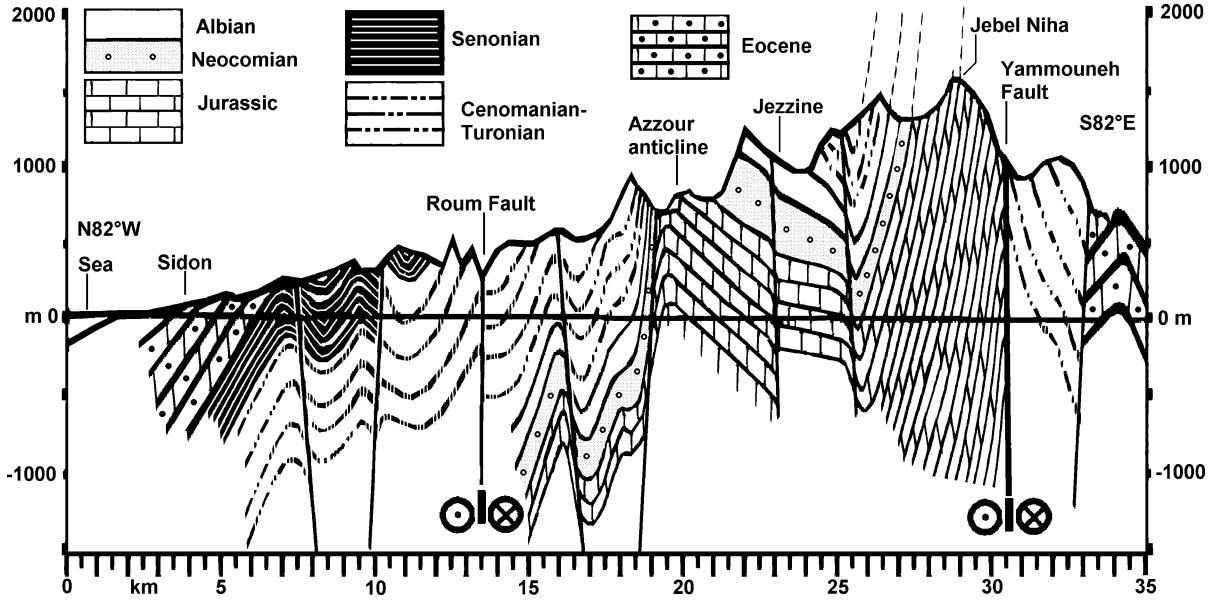

Fig. 4. Cross-section across the southern part of the Lebanon stepover, between the Mediterranean coastline and the southern end of the Yammouneh Fault (Fig. 2). Adapted from Walley (1998, Fig. 4b).

predicting all components of the model region's deformation, the most straightforward result from this analysis was a demonstration that the ratio U/V is limited by an upper bound k where

$$\cos(\theta) = k \equiv U/V. \quad (1)$$

Numerous palaeomagnetic studies (results compiled by Westaway, 1995) indicate anticlockwise rotation within these surrounding mountain ranges by ~30° since the Early Cretaceous. Westaway (1995) suggested that this rotation has resulted from distributed left-lateral simple shear across the Lebanon stepover during slip on the DSFZ. However, Walley (1998) has argued instead that some aspects of the structure of this region (including, presumably, the palaeomagnetic rotations) formed in the Late Cretaceous, during earlier deformation that was unrelated to the DSFZ.

The parameters used in Westaway's (1995) calculations require substantial revision in the light of new data. First, the new southern DSFZ Euler vector predicts (for a representative point within the Lebanon stepover, at 34°N, 36°E) AR–AF motion towards N18°W. The angle θ between this direction and the N30°E strike of the Yammouneh Fault is thus 48°, not the 32° calculated by Westaway (1995) using Garfunkel's (1981) Euler pole. Second, Walley (1998) showed from the offset of distinctive Cretaceous inliers used as piercing points, that the Yammouneh Fault has slipped left-laterally by 47 km, and estimated a further ~20 km of slip on the Serghaya Fault. The ratio of this 67 km of slip to the 105 km on the southern DSFZ indicates that k [Eq. (1)] is ~0.64. This is very close to cos(48°) or ~0.67, suggesting that the left-lateral faults in the Lebanon stepover have slipped by about the maximum distance permitted by its geometry. Westaway (1995) instead assumed, following Hancock and Atiya (1979), that the Yammouneh Fault has slipped only ~7 km.

Westaway (1995) attempted to explain the observed 30° anticlockwise rotation of Early Cretaceous magnetisation vectors in the Lebanon Mountains, from azimuth α_o 50° to azimuth α 80° (measured relative to the internal fault of the stepover), as a consequence of the distributed deformation along this stepover. He showed that this requires Ψ, the azimuth of the direction of no rotation within the distributed deformation (again, measured relative to the internal fault), to satisfy $\theta \leq \Psi < 50°$, the lower bound to Ψ requiring $k \rightarrow 0$. With θ now 48°, this assumption would thus seem to impose a tight constraint on Ψ. However, Westaway's (1995) Eq. (A31) allows one to estimate from these parameters the total shortening strain ζ in the Lebanon Mountains required to account for the observed rotation. Using Ψ=48° requires ζ to be ~12, an implausibly high value, rather than the geologically more plausible value of ~2 deduced by Westaway (1995). Furthermore, Ψ=48° would require minimal left-lateral slip ($k \rightarrow 0$), conflicting with the many tens of kilometres of left-lateral slip now documented. Conversely, if this internal fault is slipping at the maximum rate permitted by the geometry, then $k=\cos(\theta)$, such that, using Westaway's (1995) Eq. (A29), Ψ is 90°. Ψ=90° is also suggested by the geometry of the folds in the Lebanon Mountains, which trend parallel to the Yammouneh Fault (Griffiths et al., 2000), indicating shortening in the perpendicular direction. With Ψ=90° rather than 48°, Westaway's (1995) Eq. (A31) simplifies to $\zeta=\tan(\alpha_o)/\tan(\alpha)$, thus requiring $\zeta<1$, indicating that extension (not shortening) would be required. This is because distributed shortening with Ψ=90° will cause a vector with α_o=50° to rotate clockwise, not anticlockwise. Walley's (1998) intuitive conclusion, that such large rotations cannot have been associated with slip on the DSFZ, is thus entirely supported by the new data and analysis. Westaway's (1995) analysis indeed indicates that, in the limit of k being as large as possible, the strain rate for distributed simple shear across a stepover is 0. Structural trends (or embedded magnetisation vectors) still experience some rotation, due to the flattening effect of the component of distributed shortening perpendicular to the internal fault: but any resulting rotation is likely to be small. It is presumed that this component of distributed crustal shortening is being accommodated by thickening of the brittle upper crust, requiring surface uplift. However, as a result of this surface uplift, the upper part of the crustal column is presumed to have been eroded, thus explaining why older rocks are typically exposed along the Lebanon stepover (e.g., Walley, 1998). Their observed typical outward tilting (Fig. 4) can also be readily explained as a consequence of a tapering in the crustal shortening strain rate away from the DSFZ.

The Quaternary slip rate on the Yammouneh Fault in southern Lebanon can be tentatively estimated from its ~3.5 km left-lateral offset of the Litani River near

Marjayoun (Fig. 2). It is widely observed, both in the Arabian platform (e.g., Westaway and Arger, 1996; Bridgland et al., 2003) and elsewhere (e.g., Westaway, 2002c,d), that river gorges typically became entrenched around ~0.9 Ma, due to the widespread increase in rates of uplift and incision that occurred at that time, possibly because of effects of climate causing increased rates of erosion, leading to increased rates of vertical crustal motion as the isostatic response (e.g., Westaway, 2002b,c,d). Equating this timing with oxygen isotope stage (OIS) 22, at 870 ka, the first very severe Quaternary glaciation, the resulting slip rate estimate is 4.0 mm a^{-1}.

The geomorphology, and trenching, along the southern part of the Serghaya Fault around Zabdani (Fig. 2) indicate a Holocene slip rate of ~1 mm a^{-1}, and possibly as high as ~2 mm a^{-1} (Gomez et al., 2001a,b). Such a rate can account for Walley's (1998) estimate of ~20 km of total left-lateral slip on this fault. Walley (1998) proposed that this component of slip dies out in distributed shortening across the Palmyra fold belt farther north and east in Syria. Estimates of the total shortening within this fold belt range from ~20 km (Chaimov et al., 1990) to ~30 km (Khair et al., 1997). However, Walley (1998) argued that, as in Lebanon, some of the structure of the Palmyra fold belt predates the DSFZ, so the total of its syn-DSFZ shortening in it is less. Consistency between the relatively high slip rate indicated on the DSFZ in Syria by trenching (Meghraoui et al., 2001, 2003; Meghraoui, 2002) and other evidence suggests that no significant component of AF–AR plate motion is currently being "absorbed" in the Palmyra foldbelt, suggesting that its folding has been a consequence of a different geometry of plate motions, earlier in the evolution of the DSFZ (see below).

Past studies have suggested that the Roum Fault has taken up many tens of kilometres of left-lateral slip (e.g., Girdler, 1990; Butler et al., 1998). However, they have been superseded by work by Griffiths et al. (2000), which shows that a maximum observed total of ~5.7 km of localised left-lateral slip and ~1.5 km of associated distributed left-lateral simple shear have occurred near the southern end of this Fault where it offsets the Litani River (Fig. 2), suggesting a time-averaged slip rate of ~0.5 mm a^{-1}. Griffiths et al. (2000) also showed that the slip on the Roum Fault dies out gradually northwards over tens of kilometres distance, presumably due to the component of distributed shortening revealed by the folding in the block between it and the Yammouneh Fault (Fig. 4).

2.2. The Homs area, western Syria

North of the Lebanon–Syria border, much of the land surface is covered by the Late Miocene–earliest Pliocene Homs Basalt (Fig. 5). The local DSFZ segment, the Masyaf Fault—the end-on continuation of the Yammouneh Fault—trends almost due north, transecting this basalt outcrop (e.g., Trifonov et al., 1991) (Fig. 5).

Walley (1998) has suggested that the Serghaya Fault also continues NNE into Syria, past Al Qusayr and SE of Homs, before splaying in the vicinity of Furqlus and Abu Qatur (Fig. 2) into the Jhar and Bishri faults within the Palmyra Foldbelt. However, geological mapping in the vicinity of Al Qusayr (e.g., Kozlov et al., 1963; Ponikarov et al., 1967) has revealed no evidence of any such fault (Fig. 5), and none has been noted during recent fieldwork in this area (Bridgland et al., 2003). Furthermore, the established geological mapping of Syria (e.g., Ponikarov et al. (1967) instead shows the Jhar and Bishri faults linked to the DSFZ a long way farther south—in the Syria–Lebanon border area SW of Damascus (Fig. 2). The active slip on the southern part of the Serghaya Fault (Gomez et al., 2001a,b) (observed around Zabdani; Fig. 2) thus evidently dies out northward within the Lebanon stepover, and does not continue northeastward into Syria (contra Walley, 1998). Nonetheless, most outcrop in the Homs area is Pliocene and Quaternary (e.g., Dubertret and Vautrin, 1938; Bourcart, 1940; Kozlov et al., 1963) (Fig. 5), so it is conceivable that a northward continuation of the Serghaya Fault could have been active in the Miocene but slip on it has since ceased.

Previous studies (e.g., Westaway, 1994, 1995; Brew et al., 2001) have assumed that the Masyaf Fault is a transform fault segment. However, the structure of the DSFZ in Syria is similar (albeit on a smaller scale) to that in Lebanon; that is, Cretaceous and Jurassic rocks are exposed along the Masyaf Fault (Fig. 5). They also tilt away from it on both sides (Figs. 5 and 6), although this tilting is asymmetric—it persists for >~40 km to the west (Fig. 6), but dies out within ~20 km to the east (Fig. 5). Furthermore, the

Homs Basalt is deposited on an erosion surface that is now tilted away from the DSFZ (Fig. 6), in the same sense as but at a lower angle than the underlying structure is tilted. It can be presumed that this surface was subhorizontal at the time of basalt eruption; thus, much of this structural tilting occurred before ~5 Ma

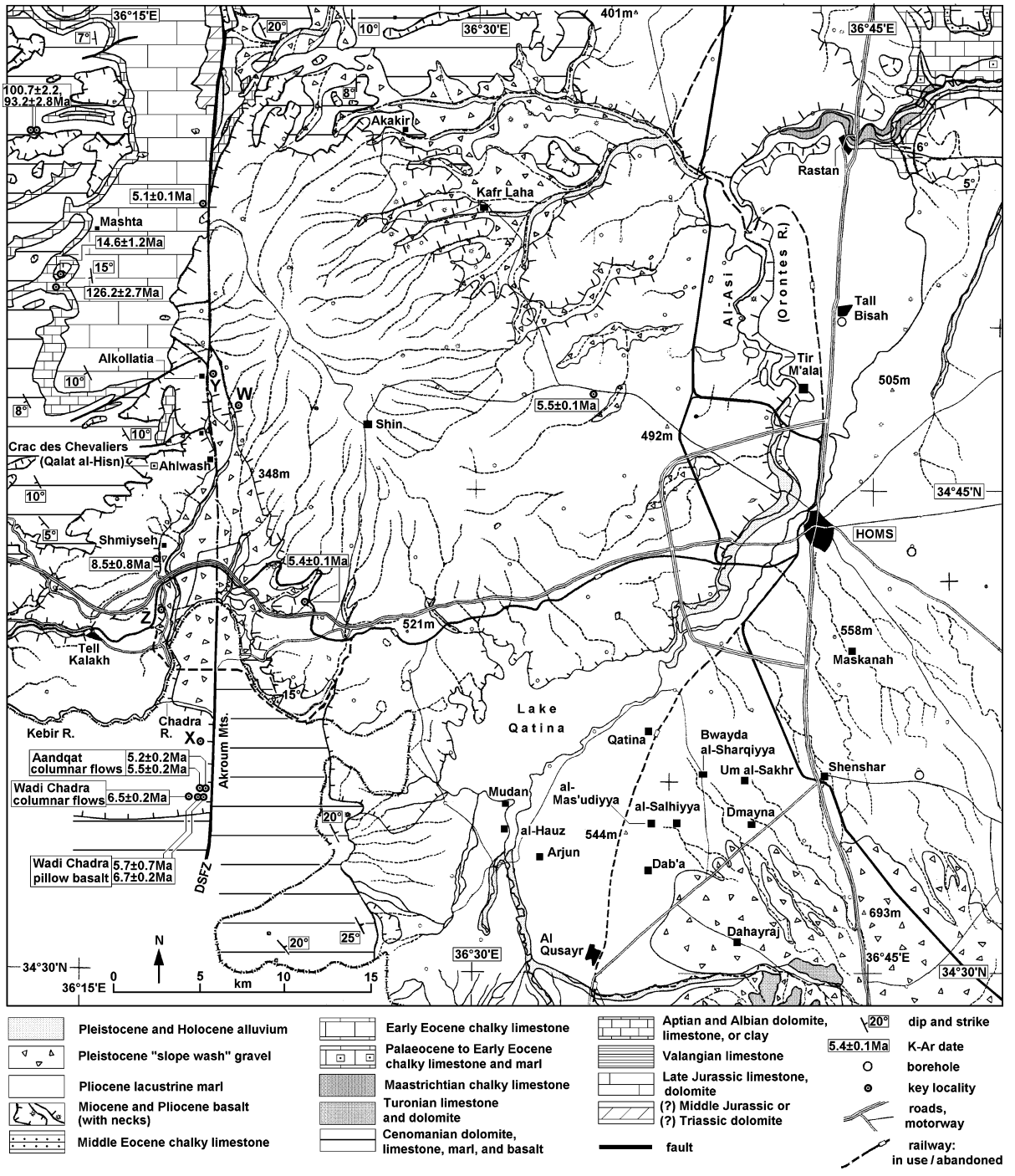

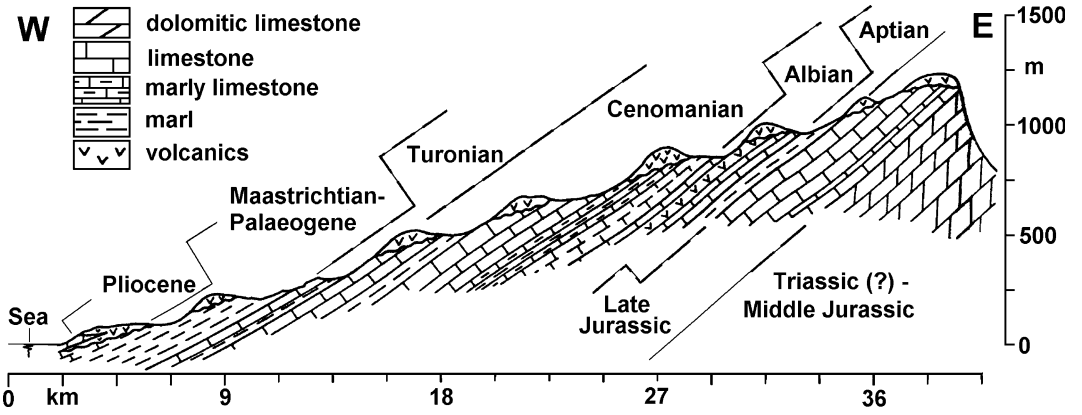

Fig. 6. East–west cross-section located ~5 km north of Mashta (Figs. 2 and 5), showing the disposition of Miocene basalt in relation to the Mesozoic sedimentary sequence. Adapted from Mouty et al. (1992, Fig. 5). Compare with Fig. 4.

but some of it has occurred since, suggesting (by analogy with Lebanon) that this tilting is the result of distributed crustal shortening and thickening at a rate that decreases away from the DSFZ. By analogy with Lebanon (Fig. 4), it can thus be argued that this part of the DSFZ is also a stepover—although at a more acute angle than in Lebanon. This interpretation is consistent with the revised DSFZ Euler vector, which requires relative plate motion towards N21°W in this part of Syria, making θ~21°: less than the ~48° value typical in Lebanon, but still significant.

West of Homs (at 34.7°N, 36.3°E), the 0.385° Ma^{-1} AF–AR relative rotation rate predicts relative motion at 6.57 mm a^{-1} towards N21°W. This requires a slip rate no greater than 6.57 mm $a^{-1}\times\cos(21^\circ)$ or 6.13 mm a^{-1} on the Masyaf Fault, predicting ~31 km of slip since 5 Ma. The 0.42° Ma^{-1} rate predicts a slip rate no greater than 6.68 mm a^{-1}, with ~33 km of slip since 5 Ma. An important constraint on the present-day kinematics is now provided by trenching at El Harif, ~5 km north of Masyaf town (Meghraoui et al., 2001, 2003; Meghraoui, 2002). The DSFZ has particularly simple form in this locality, with only a single active strand, which offsets an aqueduct—of Hellenistic or Roman origin—by 13.6 m. This trenching indicates that this structure has been offset by three earthquakes. The first of these, involving a 4.5-m offset, seems to have occurred not long after the aqueduct was built, being radiocarbon dated to no older than 210 BC. Radiocarbon dating also indicates that the final event occurred just under 1000 years ago, enabling it to be associated with the destructive historical earthquake of 29 June 1170 (e.g., Ben-Menahem, 1981; Ambraseys and Barazangi, 1989). Earlier major earthquakes are known on the DSFZ in Syria, for instance in AD 859, 500, 245 and 115, and 63 BC (e.g., Ben-Menahem, 1981), but it is unclear at this stage which were responsible for the initial two offsets of this aqueduct. The local slip rate can thus be estimated as 13.6 m/2212 a or 6.15 mm a^{-1}. The true rate may be higher than this figure, if the first earthquake occurred well after 210 BC, or lower, if the next earthquake does not occur for centuries in the future. Meghraoui (2002) estimated that the true slip

Fig. 5. Geological map of the DSFZ and its surroundings in western Syria and northern Lebanon, adapted from Kozlov et al. (1963). Geological detail in Lebanon is simplified from Butler et al. (1997). K–Ar dates and site positions in the Chadra Valley, Lebanon, are from Butler et al. (1997) and Butler and Spencer (1999): 6.7±0.2, 6.5±0.2, 5.7±0.7, 5.5±0.2, and 5.2±0.2 Ma. K–Ar dates in Syria are from Mouty et al. (1992), the sites being located as accurately as possible using their map (their Fig. 1b) rather than their table of coordinates, some of which do not tally with the map: 8.5±0.8, 5.5±0.1, 5.4±0.1, and 5.1±0.1 Ma. The borehole shown directly east of Homs revealed basalt beneath 119-m thickness of Pliocene lacustrine marl. Approximate alignments of the modern road and railway networks have been added to facilitate location. The northward continuation of the Serghaya fault according to Walley (1998) (dotted line in Fig. 2) runs SW–NE along the NW margin of the range of hills in Cretaceous limestone south of Dahayraj, and is then projected farther NE across the Pliocene marl outcrop depicted on this map.

rate probably lies within the range ~5.5–7.0 mm a^{-1}. For instance, if the initial offset is assumed to have occurred in 63 BC, the subsequent time-averaged slip rate can be estimated as ~13.6 m/2065 a or 6.59 mm a^{-1}. Such a slip rate is roughly consistent with the estimated upper bound to the AF–AR rotation rate in this study, of 0.42° Ma^{-1}. Meghraoui et al. (2003) estimated that this aqueduct was built between AD 30 and AD 70, and thus derived a subsequent slip rate of 6.9±0.1 mm a^{-1}, suggesting an AF–AR rotation rate of 0.434±0.006° Ma^{-1}.

Many studies have noted that the Homs Basalt has an apparent left-lateral offset (Fig. 5). This offset was estimated as ~20 km by Quennell (1984); others have since quoted a range of smaller values. However, studies have argued in contrast that this part of the DSFZ ceased to be active in the latest Miocene or earliest Pliocene (e.g., Girdler, 1990; Butler et al., 1997, 1998; Butler and Spencer, 1999). As already noted, others (e.g., Brew et al., 2001) have argued instead that this part of the DSFZ did not become active until the Pliocene. These hypotheses are, of course, contradictory, and this point requires resolution.

Girdler (1990) argued that the northern DSFZ can be regarded as inactive because of an apparent lack of seismicity. He noted microearthquakes located along the line of the Roum Fault, and thus deduced that active slip continues northward along this line and a hypothetical offshore northward continuation. However, this possibility can now be excluded as a result of detailed study of the Roum Fault (Griffiths et al., 2000), as well as the lack of evidence for this hypothetical offshore fault zone (e.g., Yurtmen et al., 2002). The microseismicity west of the main DSFZ strand in Lebanon can instead be readily explained as a result of the distributed crustal deformation occurring along the Lebanon stepover (Westaway, 1995; Griffiths et al., 2000). Of course, the absence of seismicity along the Yammouneh Fault and the northern DSFZ in recent decades does not mean that these structures are inactive; as already noted, these fault segments have experienced many large historical earthquakes.

Butler et al. (1997) argued that the northern DSFZ has not slipped since the latest Miocene/earliest Pliocene using field evidence from northern Lebanon (Figs. 5 and 7). In northernmost Lebanon, the DSFZ follows the valley of the Chadra River, which flows northward—west of the Akroum mountain range—into the Al-Bugeia lake basin on the Syrian border. In this vicinity, subhorizontal basalt flow units are directly juxtaposed along the DSFZ on its western side. Butler et al. (1997) also reported that in the Chadra valley the DSFZ can be easily identified by a zone of fracturing, with ~10–15 m width of fault gouge-indicating intense cataclasis—directly abutting the eastern margin of the basalt (Fig. 7). They also reported that this fault gouge is made entirely of limestone fragments, no basaltic material being found within it. They thus concluded that this fault has not slipped since the basalt erupted, such that the subvertical contact between this basalt and the fault gouge is a dipping unconformity.

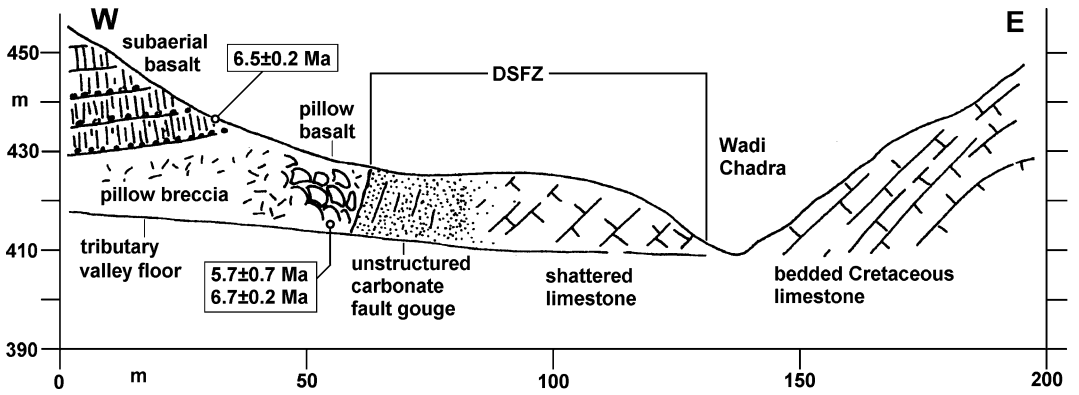

Fig. 7. Cross-section across the DSFZ in northernmost Lebanon, adapted from Butler and Spencer (1999, Fig. 5) (see also Butler et al., 1997, 1998) showing the northern end of the active Yammouneh Fault in the Wadi Chadra valley in northernmost Lebanon (Fig. 2). See text for discussion.

This interpretation by Butler et al. (1997) thus requires that the western margin of the fault gouge was an exposed subvertical face before the basalt erupted, which seems unlikely. The absence of basalt clasts in the fault gouge can anyway be explained for a number of reasons. First, limestone overwhelmingly comprises the preponderant rock type in this region. In comparison, the volume of basalt is small. Second, it is evident that much of the Homs basalt has experienced severe alteration, due to prolonged chemical weathering. Any loose clasts within the fault gouge, derived originally from this basalt, may thus have since disintegrated as a result of this process. Third, where intact, basalt is stronger than limestone. Thus, once the basalt was initially cut by left-lateral faulting, subsequent slip would be expected to be concentrated within the limestone, not within the basalt, making it difficult for basalt clasts to enter the fault gouge.

The disposition of Homs Basalt flow units relative to the DSFZ can also be observed at many localities in western Syria. Outside the linear valley that follows the DSFZ, these flow units are invariably subhorizontally bedded, reflecting the very gentle tilting away from the DSFZ of the land surfaces on which they were deposited (Fig. 6). However, along the flanks of this valley, where these flow units are clearly exposed they can be observed to be dipping inward towards this valley. That is, they are indeed often observed to be interbedded with sloping palaeosols or other slope deposits. This geometry is particularly clear along the western (African) side of the Masyaf Fault south of Shmiyseh, just north of the Lebanon border (Z in Figs. 5 and 8a), where the basalt section has been exposed by quarrying, and on its eastern (Arabian) side around Alkollatia (Y in Figs. 5 and 8b and c), where a section through the sloping basalts and interbedded palaeosols has been exposed during recent construction of an irrigation canal. This is clear evidence that this linear valley already existed at the time of eruption of the Homs basalt, which means that the DSFZ predates this eruption. This evidence differs from what Butler et al. (1997) observed in northern Lebanon, where the basalt abutting the Chadra valley from the west is subhorizontal (Fig. 7). However, they noted that the older basalt flow unit in this area is pillowed, indicating a subaqueous eruption, which does imply the existence of a localised topographic depression at this time.

The fact that the northern DSFZ predates the Homs Basalt is also clear from consideration of relationships between slip rates and total offsets. For instance, the present kinematic model predicts an upper bound to the slip rate in the range ~6.2 mm $a^{-1} \times \cos(48^\circ)$ to ~6.8 mm $a^{-1} \times \cos(48^\circ)$, or ~4.1 to ~4.6 mm a^{-1}, on the Yammouneh Fault in north-central Lebanon. At a uniform slip rate, the 47 km of total slip on this fault, estimated by Walley (1998), requires its age to be ~47/4.6 to ~47/4.1 or ~10–11 Ma. It can thus be presumed that, early in the evolution of the DSFZ, from ~19 Ma until at least 11 Ma, a significant component of the relative plate motion was accommodated instead by slip on the faults east of the Yammouneh Fault, plus shortening in the Palmyra foldbelt (Fig. 2). It remains unclear whether the switch to the modern geometry occurred gradually or abruptly, but the evidence suggests that this change occurred well before the eruption of the Homs Basalt—in the late Middle Miocene or early Late Miocene.

As already noted, estimating the amount of left-lateral slip since ~5 Ma from the disposition of the Homs Basalt is problematic. The fact that its linear valley existed before the basalt was erupted, such that many flows entered this linear valley from either side, means that one cannot simply correlate any individual flow from one side of this fault zone to the other. In addition, the fact that this linear valley already existed means that one cannot assume that equivalent relief existed at any locality on both sides of the fault at the time of basalt eruption. It is therefore not possible to derive any particular precise slip estimate from the Homs Basalt. A more pertinent issue is whether there is any evidence from the vicinity of the Homs Basalt to contradict the ~31–33 km of slip estimated since the end of basalt eruption at ~5 Ma, or the ~40–43 km estimated since its start at ~6.5 Ma. The answer at this stage is clearly no, and it will take a vast programme of fieldwork in this region to settle this point with any greater precision.

2.3. The Ghab Basin in northern Syria and its surroundings

The Ghab Basin is revealed by a Quaternary alluvial plain at ~100 m altitude, ~60 km long (N–S)

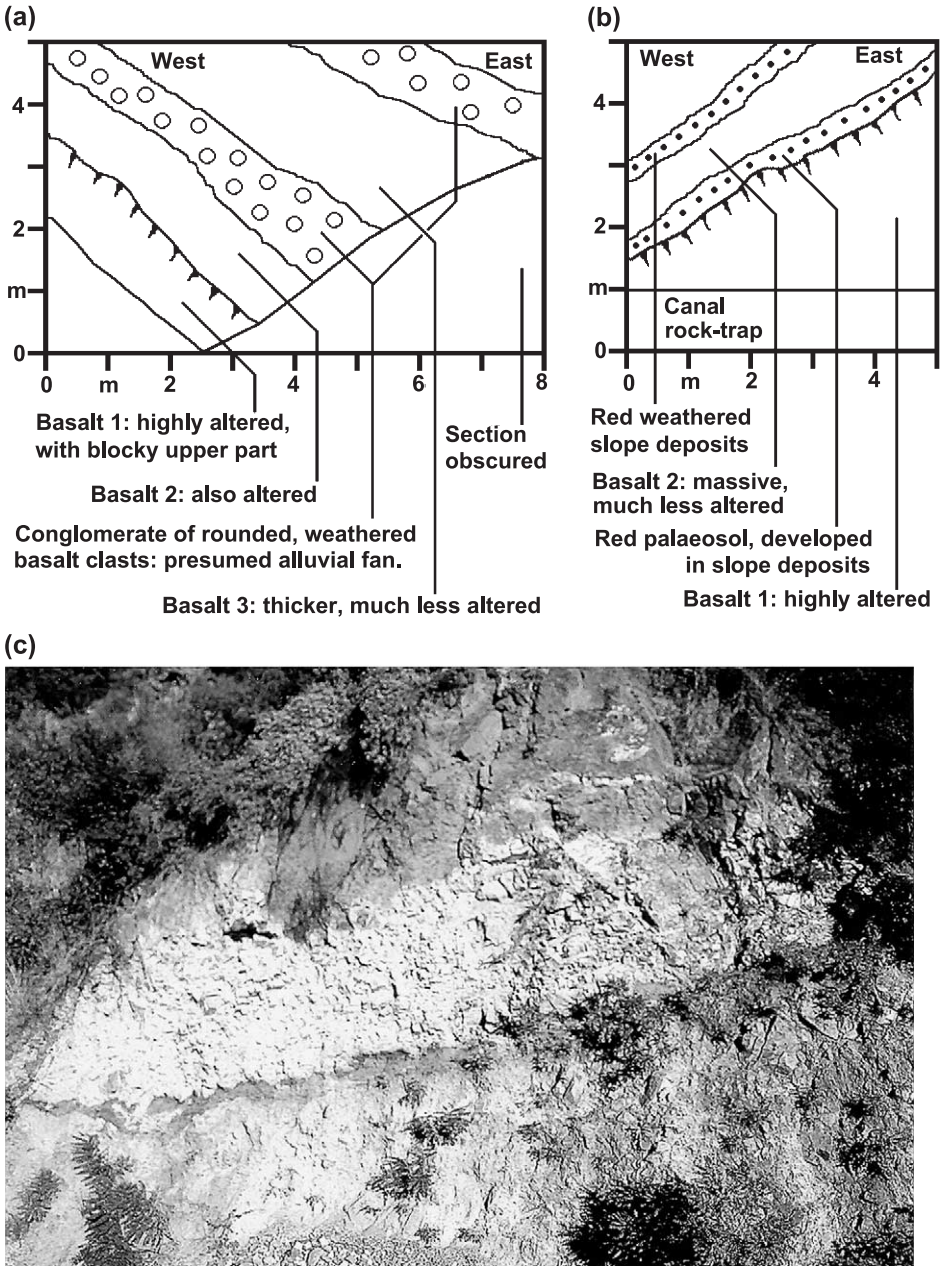

Fig. 8. (a) Cross-section exposed in the western margin of the DSFZ linear valley south of Shmiyseh, just north of the Lebanese border, at [BU 5284 4174] (Z in Fig. 5). (b) Cross-section exposed in the eastern margin of the DSFZ linear valley east of Alkollatia (Y in Fig. 5), at [BU 5501 5477]. (c) Field photograph at part b. The palaeosol separating the two basalt flows appears dark. Observed in September 2001, these are example localities indicating that during the Homs Basalt volcanism, basalt flows cascaded into the DFSZ linear valley from both sides, thus demonstrating that this valley already existed at the time.

and ~10 km wide, located on the northern DSFZ (Figs. 2 and 3). Both its margins are bounded by left-lateral faults (e.g., Trifonov et al., 1991) (Figs. 2 and 3). The escarpment at its western margin, which forms the eastern flank of the Jabal Nusayriyah or Coastal Mountains, across which the land surface rises to up

to 1562 m, is the more prominent. Like farther south (Figs. 5 and 6), the Mesozoic mainly carbonate sequence is exposed along both escarpments (Fig. 3). Along both flanks these rocks are folded, pervasively broken up by minor faulting, and typically tilted away from the line of the DSFZ (e.g., Brew et al., 2001). The escarpment to the east is mostly in Cretaceous rocks, with some Tertiary cover still preserved on top (Fig. 3). To the west, the more dramatic deformation has exposed much of the Jurassic sequence, with the Cretaceous preserved on top, but with almost all the former Tertiary cover eroded.

Previous studies (e.g., Matar and Mascle, 1993; Westaway, 1994; Brew et al., 2001) have regarded the Ghab Basin as a pull-apart basin located at a leftward step between transform fault segments of the DSFZ. It indeed gives the strong impression of the classic "rhomb" pull-apart basin shape (Fig. 2), as many global studies of strike-slip faulting (and, most recently, Brew et al., 2001) have noted. This study will suggest a fundamentally different interpretation, which is consistent with the proposed kinematics of the rest of the DSFZ. That is, the Ghab Basin owes its existence to the local component of extension across a splay in the DSFZ, which is located within a transpressional stepover. This interpretation thus resembles the overall geometry deduced by Westaway and Arger (1996) for the smaller Gölbaşı Basin on the EAFZ (Figs. 1 and 2).

Satellite images (e.g., Muehlberger and Gordon, 1987; Perinçek and Çemen, 1990) and local mapping (e.g., Shatsky et al., 1963; Ponikarov et al., 1966) indicate that the DSFZ splays in the vicinity of the Ghab basin (Figs. 2 and 3). Its western strand, for which I suggest the name Nusayriyah Fault, follows the western margin of this basin, trending almost due N–S. Its eastern strand follows the eastern margin of the southern two-thirds of the basin (south of locality N in Fig. 3), before heading off towards N10°E (Fig. 2). I suggest the name Apamea Fault for the fault that bounds the eastern margin of the Ghab basin and continues for ~20–25 km northward to a separate Quaternary depocentre—the ~24-km-long and up to ~5-km-wide Rouj Basin (the "Balou Trough" of Brew et al., 2001) (Fig. 3). The proposed component of local extension that has created the Ghab Basin thus results from the component of northward divergence between these fault strands.

Farther north, the topography, geomorphology, geological mapping (e.g., Ponikarov et al., 1966), and satellite image interpretation (e.g., Muehlberger and Gordon, 1987; Perinçek and Çemen, 1990) suggest that four significant distinct faults are present. One forms a northward end-on continuation of the Nusayriyah Fault along the western flank of the Orontes valley, before disappearing beneath the Holocene sediment of the Amik Basin across the Turkish border. I suggest the name Qanaya–Babatorun Fault for this structure, named after the largest villages along it (Fig. 3). The southern margin of outcrop of Pliocene marine sediment in the Orontes valley is offset left-laterally across this fault by ~10 km (I–J in Fig. 3). This marine sediment formed in the earliest Pliocene, when the Mediterranean Sea briefly flooded this area (e.g., Ponikarov et al., 1967) following the Messinian regression before 5.3 Ma. At both these suggested piercing points, the southern margin of the marine sediment outcrop marks the limit beyond which this sediment has not yet been eroded. As in any such instance, differential erosion would thus mean that the true amount of left-lateral slip is not being expressed (e.g., Westaway, 1999). Nonetheless, if this ~10-km apparent offset represents a true left-lateral offset, this is evidently an important active fault segment, indicating a time-averaged slip rate of ~1.9 mm a^{-1} since then. Seismic reflection profiling by Perinçek and Çemen (1990) reveals the subsurface continuation of this structure beneath the Amik Basin: it steps left and links end-on with the Amanos Fault that forms the western margin of the Karasu Valley farther north (e.g., Yurtmen et al., 2002).

The other three faults become apparent north of the Rouj Basin, suggesting that—like the Ghab Basin—it marks a splay in the faulting (Fig. 3). The easternmost of these, the Afrin Fault, continues NNE across northernmost Syria and appears to link end-on with other Late Cenozoic strike-slip faults in the Gaziantep area of southern Turkey (e.g., Coşkun and Coşkun, 2000; Yurtmen and Westaway, 2001b), notably the Kırkpınar Fault of Westaway and Arger (1996) (Fig. 9). The Armanaz Fault continues northward, past the town of this name, forming the eastern margin of an abrupt, ~700 m high, ridge formed of Eocene to Early Miocene marine sediment, then passing beneath the town of Harim and crossing the Turkish border. It can then be projected northward beneath the Holocene

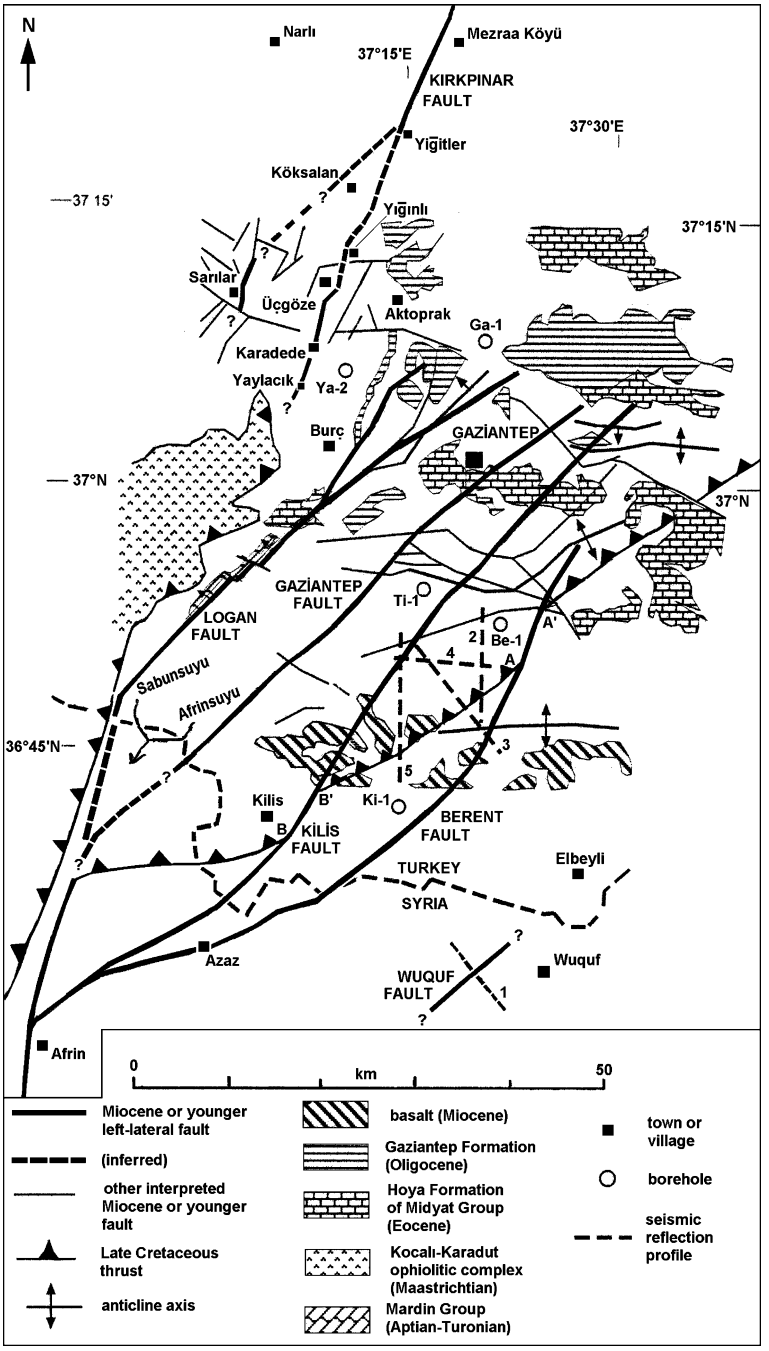

Fig. 9. Map of the Turkey–Syria border region showing Late Cenozoic strike-slip faults in relation to thrust structures dating from the latest Cretaceous ophiolite obduction and selected Tertiary depocentres. Adapted from Coşkun and Coşkun (2000, Figs. 2 and 9), also showing the Wuquf Fault from Chaimov et al. (1990) and the geometry of the Kırkpınar Fault and other information from Yurtmen and Westaway (2001b).

alluvium of the eastern part of the Amik Basin just west of Reyhanlı, before crossing back into Syria and linking end-on into the East Hatay Fault (Westaway, 1994; Yurtmen et al., 2002) that follows the line of this border northward for ~50 km (Fig. 3). It then reenters Turkey near Tahtaköprü, where the border turns east, and where it appears to be offset left-laterally by ~10 km (Eo–Co or E1–C1; Fig. 3). The fault forming the western margin of the ridge west of Armanaz is here designated as the Salqin Fault. However, as it approaches the Turkish border it becomes indistinct, and it is unclear whether it simply dies out (as shown in Fig. 3), whether it continues northward to the Amik Basin (e.g., Muehlberger and Gordon, 1987), possibly passing into the leftward step in faulting that links into the Amanos Fault, or whether it bends towards the NNE (e.g., Perinçek and Çemen, 1990), suggesting that it may merge with the northward continuation of the Armanaz Fault somewhere beneath the Quaternary alluvium west of Reyhanlı. Further fieldwork in the immediate vicinity of the Turkish–Syrian border is needed to clarify this point. However, as Yurtmen et al. (2002) have noted, it has so far proved impossible to obtain permission for such fieldwork from the authorities in either country.

Subsequent fieldwork has shown that the tentative suggestion by Westaway and Arger (1996), that faulting steps to the right near Tahtaköprü from the East Hatay Fault to the Kırkpınar Fault along a localised transpressional stepover through the Kartal mountain range (Fig. 2), is incorrect (Fig. 9). The alternative view suggested previously, by satellite image interpretation (e.g., Muehlberger and Gordon, 1987; Perinçek and Çemen, 1990), is thus once again supported: that faulting continues NNE along the eastern margin of the Karasu Valley for another ~50 km to the vicinity of Sakçagöz. Satellite image studies (e.g., Muehlberger and Gordon, 1987; Perinçek and Çemen, 1990) and geological mapping (e.g., Terlemez et al., 1997; Yurtmen and Westaway, 2001b) (Fig. 3) indicate the presence of many discontinuous fault strands typically oriented SW–NE or SSW–NNE across a broad zone in this region. This structural trend originally developed in this region as a result of the latest Cretaceous ophiolite obduction (e.g., Tolun and Pamir, 1975). In many cases, it is difficult to determine whether any given structure with this trend in this region simply dates from that time or has been reactivated. However, it is evident that some structures with this trend in this region have been reactivated in the Neogene (e.g., Terlemez et al., 1997; Coşkun and Coşkun, 2000; Yurtmen and Westaway, 2001b; Fig. 9). The local situation thus appears to resemble that reported farther south along the DSFZ (e.g., Lovelock, 1984; Walley, 1998), with some Late Cenozoic fault segments reactivating preexisting lines of weakness. This evidence suggests that a substantial proportion of the left-lateral slip since the DSFZ became active may step to the right across the limestone uplands north of the Kartal Mountains, and then along the western margin of the uplands of the Gaziantep Plateau east of Narlı and Pazarcık, linking the East Hatay Fault to the Kırkpınar Fault and/or the EAFZ in the Gölbaşı area (Fig. 2).

Gravity and seismic reflection prospecting indicate that the Ghab Basin fill is up to ~1700 m thick (Brew et al., 2001). It consists almost entirely of Pliocene lacustrine sediment, the clastic component being derived from the Orontes River (Fig. 2); typically, only a thin veneer of Quaternary sediment is present (e.g., Besançon and Sanlaville, 1993; Domas, 1994). Furthermore, drilling (into a limited number of localities on the basin flanks and one structural "high" in the basin interior) has revealed no Miocene fill between the Pliocene sequence and Eocene or Mesozoic bedrock (Brew et al., 2001). Interpretations of seismic reflection profiling (Brew et al., 2001) also suggest that there is no Miocene fill throughout the Ghab Basin, although this deduction is not confirmed elsewhere by drilling.

Brew et al. (2001) regarded this apparent absence of Miocene sediment as strong grounds for their interpretation that the northern DSFZ did not become active until the Pliocene. It is suggested below that the best estimate for the age of the EAFZ is ~4 Ma. It can thus indeed be presumed that the modern geometry of faulting in northern Syria, which links end-on to the EAFZ via the Armanaz Fault and East Hatay Fault (Fig. 2), is no older. Brew et al. (2001) also deduced that the outward tilting of the Mesozoic sequence, beyond both flanks of the DSFZ, developed before the DSFZ became active—this fault zone developing later along the N–S axis of this preexisting anticline. However, it was suggested earlier from the disposition

of the Homs basalt that part of the equivalent tilting farther south has developed since the start of the Pliocene, implying that it has accompanied the Plio-Quaternary phase of slip on the DSFZ, presumably accommodating the required component of distributed shortening in its surroundings. It is suggested here that essentially the same geometry has existed across the Ghab Basin. That is, the required component of distributed shortening and thickening, at a strain rate that increases towards the DSFZ from both sides, is causing the outward tilting observed on both sides.

A test of this interpretation is provided by the disposition of the Early Pliocene marine sediment, which provides an indication of the amount of uplift in each locality since deposition. This sediment is typically found at up to ~300 m altitude (e.g., Tolun and Erentöz, 1962; Yurtmen et al., 2002), but crops out at up to ~600 m, instead, west of the Qanaya–Babatorun fault—south of Babatorun in southernmost Turkey and around Qanaya in Syria (Fig. 3). Investigations of the Orontes terrace sequence (Bridgland et al., 2003) reveal—in contrast—no more than ~400 m of uplift since the latest Miocene/earliest Pliocene along reaches of this river (between Al Qusayr and Latamneh; Fig. 2) that are several tens of kilometres east of the DSFZ. This uplift, which does not vary measurably with position along this reach of the Orontes (Bridgland et al., 2003; see also e.g., Dodonov et al., 1993; Besançon and Sanlaville, 1993), is interpreted as regional uplift: it is in localities that are east of the local tilting observed along the flanks of the DSFZ. One can thus presume that the ~600 m of uplift observed in the immediate vicinity of the DSFZ reflects this ~400 m of regional uplift plus an additional ~200-m local component of surface uplift caused by local crustal thickening to accommodate the distributed shortening along this transpressional segment of the DSFZ. It thus follows that local distributed crustal shortening and thickening have been significant in the immediate vicinity of the DSFZ during at least part of the time scale since the Early Pliocene (contra Brew et al., 2001).

Furthermore, the existence of splays in the faulting (Figs. 2 and 3) means that the deduction by Brew et al. (2001), that the Ghab Basin did not exist in the Miocene (which is itself equivocal due to the limited borehole control), does not mean that no strand of the northern DSFZ existed then. The relative motion between the African and Arabian plates in the Miocene could instead have been accommodated on the Apamea Fault and its in-line continuations to the north, which required no leftward step in the faulting. The geometry of left-lateral faulting could have changed in the Early Pliocene, with some (possibly, most) of the subsequent slip accommodated on the Nusayriyah and Qanaya–Babatorun faults instead (which did require a leftward step). Other explanations for the apparent lack of Miocene sediment in the Ghab Basin can also be envisaged. For instance, first, the present course of the middle and upper Orontes into the Ghab Basin developed in the earliest Pliocene (e.g., Bridgland et al., 2003). The absence of significant fluvial sedimentation in the Ghab Basin in the Miocene may thus reflect the absence of any major river flowing into this basin at the time. Second, throughgoing drainage along the linear valley between the Ghab and Rouj basins may have existed in the Miocene, before they became isolated by the local Pliocene volcanism (Fig. 3). If the Rouj Basin already existed and was at a lower level at the time, little or no deposition would be expected in the Ghab Basin.

During the Late Pliocene, the northern Ghab Basin was affected by basaltic volcanism (e.g., Besançon and Sanlaville, 1993; Domas, 1994) (Fig. 3). Basalt flowed westward into this lake basin, ponding it near its northern outlet around the town of Jisr ash–Shugur (Fig. 3). The subsequent surface uplift has led to the relatively easily eroded Miocene and Pliocene sediment north of this point along the Orontes valley becoming dramatically incised. However, the strength of this basalt "dam" allowed lacustrine sedimentation to continue for a time farther upstream (Domas, 1994)—the youngest lacustrine sediment in the Ghab Basin being biostratigraphically dated to Astian (i.e., latest Pliocene; ~2 Ma) age (Besançon and Sanlaville, 1993). The subsequent development of this basin (involving minimal sedimentation or erosion) may simply relate to the slow progressive partial incision by the Orontes through the upper part of this basalt "dam"—it does not require a change in the regional kinematics.

It was earlier suggested that the total slip on the Amanos Fault is ~45–50 km from the offset of the southern margin of the Hatay ophiolite (F–G or F–H in Fig. 3). Earlier discussion also suggests that the present geometry involves slip on the Amanos Fault stepping

to the left, across the Amik Basin at its southern end, onto the Qanaya–Babatorun and Nusayriyah faults, with slip then again stepping to the left across the Ghab Basin. However, if the Ghab basin did not exist beforehand, this geometry can only have existed since the Early Pliocene. The ~10 km of apparent slip since the Early Pliocene on the Qanaya–Babatorun Fault (I–J in Fig. 3) could thus reflect the total slip on this structure. If so, the bulk of the ~45–50 km of slip on the Amanos Fault must have occurred in the Miocene, but continued south on another fault strand. It is thus possible that in the Miocene, the main southward continuation was the Salqin Fault, not the Qanaya–Babatorun Fault (Fig. 2).

On the other hand, the lengths of other pull-apart basins and splay basins on the strike-slip faulting in the Eastern Mediterranean region do roughly match the total slip on the adjoining faults. Examples are the Gölbaşı Basin on the EAFZ (Westaway and Arger, 1996); the Hazar Basin on the EAFZ (see below); the Ovacık Basin on the Malatya–Ovacık fault zone (Westaway and Arger, 2001); and the Marmara Basin on the NAFZ (Westaway, 1994; Armijo et al., 1999). If this "rule of thumb" is applied to the faulting in northern Syria, the ~24-km length of the Rouj Basin would provides a rough indication of the combined slip on the Salqin and Armanaz faults. If the total slip on the Armanaz Fault is assumed to match the ~10 km on the East Hatay Fault, its apparent end-on continuation, the amount on the Salqin Fault can thus be estimated as ~14 km. The substantial width of its "rhomb" shape means that the ~60 km length of the Ghab Basin will overestimate the slip on the Nusayriyah Fault; the ~45-km lengths of its N–S trending margins provides an effective upper bound. Other slip estimates can be obtained by considering the geometry of the different splays in this faulting. Restoring 40 km of slip on the Nusayriah Fault would juxtapose point N (Fig. 3), where the Apamea Fault now bends NNE away from the Ghab Basin, against this basin's southern end, thus "closing" the basin. This is thus an effective upper bound to the slip on the Nusayriyah Fault. Point P (Fig. 3) indicates a best estimate of the point at which the Armanaz Fault splays from the Afrin Fault. The maximum feasible slip restoration would appear to place this point initially adjacent to the bend in the Apamea Fault at point N, ~25 km SSW, thus indicating the combined slip on the Salqin and Armanaz faults. The total slip on the Afrin Fault is not estimated by this reasoning. However, the relatively subdued relief (no more than ~200 m at most) across the escarpment along it between the Rouj Basin and the Ad Dana area on what is expected from the geometry to be transpressional stepover (Fig. 3) suggests that it may have not slipped as far as the other fault segments.

These upper bounds to the combined total of slip on the Nusayriyah, Salqin, and Armanaz faults of ~65 km roughly match the combined upper bounds of ~60 km on the Amanos (~50 km) and East Hatay (~10 km) faults. The partitioning of slip thus indicated suggests that significant slip (at least ~10 km) has indeed stepped leftward from the Amanos Fault to the Salqin Fault. However, ~40 km is far too much slip to have occurred on the Nusayriyah Fault to be compatible with the Pliocene age of the Ghab Basin suggested by Brew et al. (2001). It is thus evident that important issues concerning the timing of slip on individual fault segments in northern Syria, the detailed geometry of the basins along it (the respective contributions of splays vs. pull aparts), and the possibility of changes to the sense of slip, remain to be fully resolved. Such investigation will require more thorough fieldwork in this sensitive region, beyond the scope of this study.

2.4. Faulting in the Karasu Valley

As already noted, the ~200-km-long Amanos Fault appears to form, after a leftward step across the Amik Basin, a northward continuation of the Qanaya–Babatorun Fault, bounding the western margin of the Karasu Valley and the eastern flank of the Amanos Mountains (Figs. 2 and 3). As summarised by Yurtmen et al. (2002), the literature on this fault contains a great diversity of views as to its slip sense (whether mainly left-lateral or mainly normal faulting), slip rate (estimates range from a few tenths of 1 mm a^{-1} to many millimetres per year), and overall role in the regional kinematics. To help resolve this contention, Yurtmen et al. (2002) undertook K–Ar dating of basalts that have flowed from the Amanos Mountains into the Karasu Valley and are offset left-laterally across the Amanos Fault by measured distances. Key sites investigated were

at Hassa, Hacılar, and Küreci (locality A in Fig. 3) and Karaçağıl, Ceylanlı, and Büyük Höyük (locality B in Fig. 3). The results indicate that the strand of the Amanos Fault between Kırıkhan and Hassa (Fig. 2) has a slip rate of ~1.0 to ~1.6 or ~1.7 mm a^{-1}. The interpretation of these results assumed, following Westaway (1994), that the DSFZ is locally a transform fault zone slipping at ~7 mm a^{-1}. Yurtmen et al. (2002) thus concluded that the Amanos Fault takes up no more than ~20% of the AF–AR motion at present.

However, the revised AF–AR Euler vector with a 0.385° Ma^{-1} rotation rate predicts ~7.3 mm a^{-1} of relative motion towards N32°W at Hassa (~36.7°N, ~36.45°E). As this is oriented at ~52° to the ~N20°E trend of the Amanos Fault, the maximum possible local rate of left-lateral slip can be estimated (using (!01)) as ~7.3 mm $a^{-1}\times\cos(52°)$ or ~4.5 mm a^{-1}. Locally, the Amanos Fault thus takes up at least ~20% (~1/~4.5) to ~40% (~1.7/4.5) of the AF–AR motion.

At present, the strongest constraint on this slip rate comes from the dating at Hacılar, to 196±6 ka (Cassignol [unspiked] K–Ar; Yurtmen et al., 2002), of a basalt flow unit that has filled a river gorge that crosses the Amanos Fault, and has since been offset by 325±25 m. The subsequent time-averaged rate of left-lateral slip has thus been 325±25 m/(196±6 ka) or 1.66±0.18 mm a^{-1}. In contrast, Rojay et al. (2001) previously dated (^{38}Ar-spiked K–Ar) the same flow unit to 80±60 ka. With this alternative date, the slip rate adjusts to between ~2 and ~15 mm a^{-1}, with a most likely value of ~4 mm a^{-1}. However, as Yurtmen et al. (2002) noted, when applied to very young basalts, their dating technique is expected to result in larger uncertainties and greater possibilities of systematic error. Most of the wide range of slip rate permitted by the Rojay et al. (2001) dating indeed indicates values that are too high to be feasible given any plausible regional kinematic model (see below). Arger et al. (2000) and Yurtmen et al. (2002) have already discussed these data sets in detail, so further discussion is not repeated here.

If it is further assumed that the East Hatay Fault developed at ~4 Ma when the EAFZ came into being, then its ~10 km of slip (Eo–Co or E1–C1 in Fig. 3) indicates a time-averaged rate of ~2.5 mm a^{-1}. When combined with the range of slip rate estimates for the Amanos Fault, at least ~60% of the predicted N20°E component of AF–AR relative motion can now be accounted for. Yurtmen and Westaway (2001b) estimated that the Kırkpınar Fault (Fig. 9) has also slipped left-laterally by ~10 km but found no geomorphological evidence of Quaternary slip along it. Its slip may thus have been concentrated during an earlier phase of development of the DSFZ. On the other hand, later discussion of the kinematic consistency of the linkage between the EAFZ and DSFZ during the present phase of deformation seems to require up to ~7 km more SSW–NNE left-lateral slip than can be accommodated on the East Hatay Fault, raising the possibility that it may have been accommodated by throughgoing left-lateral slip between the Afrin Fault, the Kırkpınar Fault, and the Gölbaşı area. It is also possible that the Afrin Fault already existed in the Miocene, but its slip at that time died out into the zone of SW–NE-trending faults in the Gaziantep area (Fig. 9). If so, this area would have formed an analogy with the contemporaneous deformation occurring in the Palmyra foldbelt (Fig. 2); that is, both having apparently developed early in the evolution of the DSFZ, apparently by reactivating much older lines of weakness in the crust that were not optimally oriented to the AF–AR plate motion, before being superseded by throughgoing left-lateral faulting. Later discussion establishes that, although both are subject to substantial uncertainty, the rates of relative motion deduced from GPS (Fig. 10a) and the geological estimates of slip rates on faults in this area are both consistent with the proposed regional kinematic model.

North of Hassa, no Quaternary basalt flows cross and are offset by the Amanos Fault. Views have differed as to whether this part of the Amanos Fault is active at a significant slip rate (e.g., Şaroğlu et al., 1992) or not (e.g., Westaway and Arger, 1996; Yurtmen et al., 2002), the latter view being supported by the more subdued relief across the fault. Many people (e.g., Şaroğlu et al., 1992) have argued that slip continues northeastward in the vicinity of Türkoğlu from the NNE-trending northern Amanos Fault onto the ENE-trending Gölbaşı–Türkoğlu Fault (Fig. 2). Unfortunately, the junction (or intersection?) between these faults is hidden

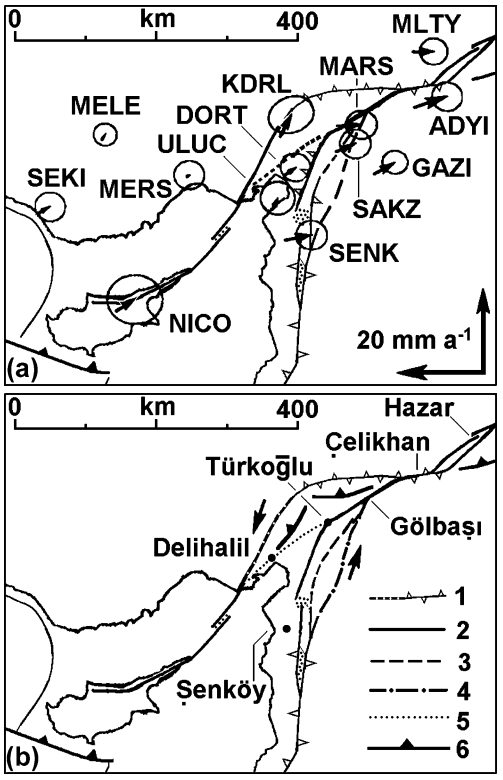

Fig. 10. Maps of the "triple junction" region between the Turkish, African, and Arabian plates. (a) Positions and motions relative to the Turkish plate of GPS points in relation to major faults, adapted from McClusky et al. (2000, Fig. 7). (b) Summary of the principal active faults in the northern part of the study region, illustrating how faulting links through the distributed boundary zone between the Turkish and Arabian plates. 1–5 indicate different fault strands within this region: the Yakapınar–Göksun and Sürgü Faults (1); the Qanaya–Babatorun, Amanos, and Gölbaşı–Türkoğlu Faults (2); the Armanaz and East Hatay Faults, and their postulated NNW continuation towards Gölbaşı (3); the Afrin Fault, and its postulated NNW continuation towards Gölbaşı (4); the Karataş–Osmaniye and Düziçi Faults, which are presumed to have been inactive since ~2 Ma (5); the suture of the southern arm of the Neotethys Ocean (6). This is not an active fault zone, except in the immediate vicinity of Çelikhan where it appears to have been locally reactivated in a left-lateral sense. The offshore Misis–Kyrenia fault zone and Kyrenia lineament in northern Cyprus may also follow this suture, locally reactivated in a left-lateral sense. However, elsewhere the active faulting avoids this suture on both sides. See text for discussion.

beneath the thick alluvium of the Aksu alluvial plain, and is thus not observable in the field. An argument against this possibility (by Westaway and Arger, 1996) holds that such an abrupt ~45° bend in strike-slip faulting (from N20°E to the N65°E strike of the western end of the Gölbaşı–Türkoğlu Fault) is not feasible, as it would require major deformation in the fault's surroundings, which is not observed. However, that view was based on the assumption that both the Amanos Fault and the Gölbaşı–Türkoğlu Fault are transform faults. Since it now seems evident that the Amanos Fault is NOT a transform fault, this kinematic objection is removed.

3. The East Anatolian Fault Zone

The left-lateral EAFZ links the northern end of the DSFZ, which previous discussion has located in the Gölbaşı–Türkoğlu area, to the NAFZ. Westaway and Arger (1996, 2001) have suggested that for most of its length the EAFZ behaves as a transform fault zone between the Arabian and Eurasian plates. The main exceptions are at its rightward steps where it crosses the Neotethys suture near Çelikhan (Fig. 10b) and farther northeast in the Gökdere Mountains near Bingöl (Fig. 1). Furthermore, Westaway and Arger (2001) noted that at its intersection with the right-lateral NAFZ near Karlıova (the notional "triple junction" between the Turkish, Arabian, and Eurasian plates), distributed deformation is required in the surroundings to one or other fault. Westaway and Arger (2001) deduced that the most likely present-day geometry involves distributed EAFZ-parallel shortening and distributed NAFZ-parallel extension in the angle between the easternmost EAFZ and the projection of the NAFZ to the east of Karlıova (see their Fig. 14a). This geometry means that at points on the EAFZ near Karlıova, less slip will have occurred than on its transform-faulting segments farther SW. The frequently quoted measurement of 22 km of total slip just SW of Karlıova (e.g., Arpat and Şaroğlu, 1972; Şaroğlu et al., 1992; Westaway, 1994) is thus expected to underestimate the total slip on the transform faulting segments of the EAFZ.

In the vicinity of the Hazar pull-apart basin, a total of up to ~35 km of left-lateral slip is evident on the EAFZ (e.g., Westaway, 1994). In this vicinity, this fault zone has two en-echelon strands (Fig. 1)—the Hazar–Şiro Fault that enters the Hazar pull-apart from the SW, and the Çüngüş Fault farther SE (Fig. 2). The

~5-km left-lateral offset of an ancient thrust fault near Hazar town (e.g., Yazgan, 1983; Michard et al., 1984) suggests 5 km of total slip on the Çüngüş Fault. The ~30-km total length of the lowlands forming the Hazar pull-apart basin (of which 21 km is occupied by Lake Hazar) suggests the total slip on the Hazar–Şiro Fault. Farther SW, near Malatya, the gorge of the river Euphrates is offset left-laterally by 13 km where it crosses the Hazar–Şiro Fault. Many studies have thus quoted 13 km as its total slip. However, it now seems clear that the incision of this gorge postdates the initiation of slip on this fault segment (e.g., Westaway and Arger, 2001).

Farther SW, the main constraint on the overall EAFZ kinematics comes from the Westaway and Arger (1996) study of the Gölbaşı Basin, where the main EAFZ strand—the Göksu Fault—splays into the WSW-trending Gölbaşı–Türkoğlu Fault and the SSW-trending fault zone that may include the Kırkpınar Fault and its en-echelon counterparts (Fig. 2). The left-lateral offset of an ophiolite body cut by the Gölbaşı–Türkoğlu Fault indicates that it has taken up ~16 km of total slip. Westaway and Arger (1996) deduced a total of 33 km of slip across the Gölbaşı basin from its geometry and from the left-lateral offset of a distinctive anticline axis used as a piercing point, thus estimating a total of 17 km of left-lateral slip at the northern end of the NNE-trending fault set that links through to this area from the south (Fig. 2).

However, as Westaway and Arger (1996) noted, this ~33-km measurement underestimates the total TR–AR relative motion due to neglecting the component of slip on the Sürgü Fault, which splays from the Göksu Fault farther northeast near Çelikhan (Fig. 2). Near Kandil (Fig. 2) the Ceyhan River flows parallel to the Sürgü Fault for ~8 km, before crossing it. However, detailed maps, such as by Perinçek and Kozlu (1983, Fig. 1) show the river ~2 km from the fault along this reach, suggesting that it is an instance of fortuitous alignment, not a true left-lateral offset. Farther east at Derbent, mapping by Perinçek and Kozlu (1983, Fig. 2) shows an ancient reverse fault, along which Palaeozoic rocks have been thrust eastward over Tertiary rocks, apparently offset left-laterally by ~4 km. This is currently the best available estimate of the total slip on this fault.

Westaway (1994) deduced from TR–AR–EU velocity vector triangle closure that the EAFZ has a slip rate of ~13 mm a^{-1}. However, his ~N10°W sense of AF–AR relative motion in this region was based on the assumption that the DSFZ in Syria is a transform fault zone, and is thus substantially in error. Revised vector triangles can be determined instead using the McClusky et al. (2000) GPS solutions for the TR–EU and EU–AR Euler vectors (1.2° Ma^{-1} about 30.7°N, 32.6°E; and 0.5° Ma^{-1} about 25.6°N, 19.7°E, respectively). These predict an EAFZ slip rate of ~8 mm a^{-1} towards an azimuth that rotates progressively concave-southward from S65°W at Hazar to S48°W at Gölbaşı (Figs. 1 and 11a and b), in agreement with the expected change in sense of relative plate motions based on field evidence (e.g., Westaway and Arger, 1996). This reduction in slip rate requires an increase in the estimated age of this fault zone from ~3 Ma (Westaway and Arger, 1996, 2001) to ~4 Ma. The slip rate on the Gölbaşı–Türkoğlu Fault can thus be estimated as ~4.0 mm a^{-1} (~16 km/4 Ma). This fault is oriented towards S75°W to the north of Pazarcık, before bending towards S65°W near Türkoğlu. For comparison, SW of Gölbaşı, all three of the tributary gorges of the Aksu River that cross the Gölbaşı–Türkoğlu Fault are offset left-laterally by ~3.5 km. Westaway and Arger (1996) suggested that the entrenchment of these river gorges which led to the rivers becoming "locked" in their courses and so progressively offset, began around OIS 22 at ~0.87 Ma. The resulting slip rate estimate is thus 4.02 mm a^{-1}, in better agreement with the EAFZ slip rate derived from the McClusky et al. (2000) GPS results than the older Westaway (1994) kinematic model. Faulting with an estimated additional slip rate of ~4.3 mm a^{-1} (~17 km/4 Ma) also splays SSW from the Gölbaşı area along a more direct line towards the East Hatay Fault (Fig. 2).

If one incorporates the published uncertainties in the McClusky et al. (2000) TR–EU and EU–AR Euler vectors, the range of possible TR–AR relative motion vectors can vary widely. For instance, at Lake Hazar it becomes ~8±2 mm a^{-1}, with possible orientations ranging from ~NE–SW to ~E–W (not illustrated). However, if one restricts discussion to solutions predicting motion subparallel to the observed faulting in this area, the uncertainty in rate is greatly reduced, to less than ~1 mm a^{-1}.

Fig. 11c depicts relative velocity vectors for the Türkoğlu area. The state of motion of the reference frame containing points located east of the Amanos Fault and south of the Gölbaşı–Türkoğlu Fault can be tentatively estimated as within the range indicated by t1 and t2 (see caption). The preferred solution is that it corresponds to t1, consistent with the view that the only relative motion between this reference frame and AR is taken up by slip at ~2.5 mm a^{-1} on the northward continuation of the East Hatay Fault. This solution predicts ~2.3 mm a^{-1} of relative motion towards S55°W across the Sürgü Fault, consistent

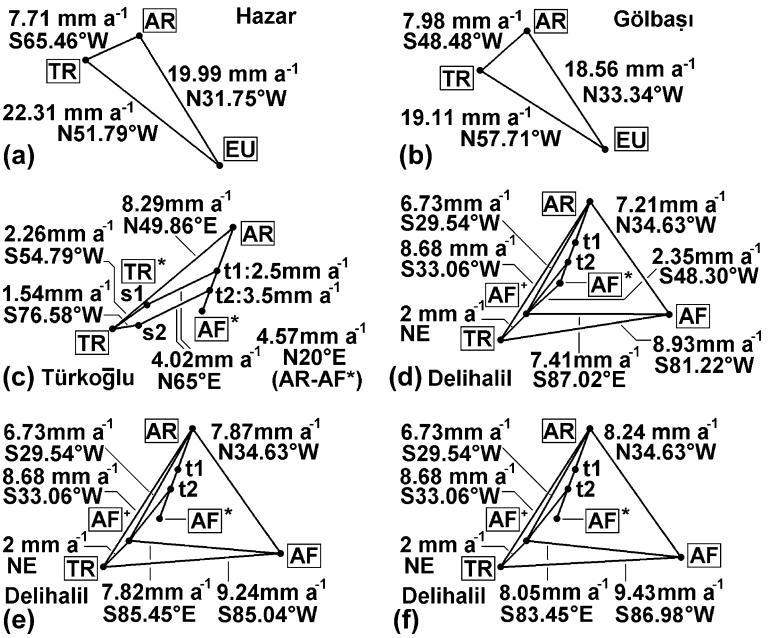

Fig. 11. Velocity vector polygons. (a) At Lake Hazar on the EAFZ (38.5°N, 39.5°E) and (b) at Gölbaşı on the EAFZ (37.8°N, 37.7°E). These are both determined by using the McClusky et al. (2000) EU–AR and EU–TR Euler vectors to predict the local TR-AR relative motion. (c) At Türkoğlu (37.4°N, 36.8°E). AF* is the reference frame moving at the maximum rate parallel to the Amanos Fault that is permitted by the geometry, given the assumed rate of AF-AR relative rotation of 0.385° Ma^{-1}. t1 and t2 are reference frames moving in this sense at 2.5 and 3.5 mm a^{-1}, respectively, representing possible choices for the state of motion of the crust east of the Amanos Fault and south of the Gölbaşı–Türkoğlu Fault. t2 represents the maximum motion relative to Arabia, for which AF* is taken as representing the state of motion directly west of the Amanos Fault, which is assumed to be slipping at ~1 mm a^{-1}—its minimum estimated rate. t1 represents the minimum motion relative to Arabia, taking account of the ~2.5 mm a^{-1} estimated slip rate on the East Hatay Fault and its northward continuations. s1 and s2 represent the corresponding states of motion of the crust north of the Gölbaşı–Türkoğlu Fault, vectors s1–t1 or s2–t2 representing the slip sense and rate on this fault (from Westaway and Arger, 1996). Vectors TR-s1 or TR-s2 thus provide estimates of the relative motion across the Sürgü Fault. Their components parallel to its E–W strike indicate rates of left-lateral slip in the range ~1.5–1.9 mm a^{-1}. The preferred solution adopts reference frames t1 and s1 for the state of motion on either side of the Gölbaşı–Türkoğlu Fault. (d) At Delihalil within the TR-AR plate boundary zone (37.0°N, 36.0°E), calculated for a rate of AF-AR relative rotation of 0.385° Ma^{-1}. AF^{+} indicates the estimated state of motion of the reference frame southeast of the Yakapınar–Göksun Fault (see text). AF*, t1 and t2 have the same meaning as in part c. No point in this vicinity is predicted to be moving with the stable interior of the African plate (AF). The calculated states of motion are instead distributed subparallel to the predicted TR–AR motion. The preferred solution is interpreted in terms of localised left-lateral slip at ~2 mm a^{-1} on the Yakapınar–Göksun Fault (TR–AF^{+}), ~2.5 mm a^{-1} on the East Hatay Fault (t1-AR), ~1 mm a^{-1} on the Amanos Fault (t2–t1), and distributed left-lateral simple shear at a rate of ~3.5 mm a^{-1} across the Amanos Mountains (AF^{+}-t2). (e) The same configuration as in part d, redrawn for a rate of AF-AR relative rotation of 0.42° Ma^{-1}. The AF–AR and AF-TR relative motion vectors are slightly longer than before, but the predicted partitioning of relative motion between TR and AR remains exactly the same. (f) The same configuration as in part d, redrawn for a rate of AF–AR relative rotation of 0.44° Ma^{-1}, consistent with the 7.0 mm a^{-1} upper bound to the DSFZ slip rate at Masyaf, estimated by Meghraoui et al. (2003). The main feature that can be used to distinguish observationally between among parts d, e, and f is that in part e, reference frame $AF^{+}$is predicted to be moving westward relative to the stable interior of the African plate ~0.4 mm a^{-1} faster than in part d, and in part f it is moving ~0.2 mm a^{-1} faster still (~8.0 against ~7.8 against ~7.4 mm a^{-1}). See text for discussion.

with a left-lateral slip rate on it of ~1.9 mm a^{-1} given its E–W strike. This predicted sense of relative motion is subparallel to the TR–AR motion. This is consistent with the overall geometry, where the Sürgü Fault splays from the EAFZ within its transpressive Çelikhan stepover (Fig. 2). If the Sürgü Fault has slipped a total of ~4 km (see above), then its age can be tentatively estimated as ~2 Ma.

NW of the EAFZ is a separate left-lateral fault system, the Malatya–Ovacık Fault Zone (MOFZ) (Fig. 1). Westaway and Arger (1996, 2001) suggested that this formed the AR–TR plate boundary when the Turkish plate first came into being with the initiation of slip on the NAFZ. At this time, the eastern end of the NAFZ was at its intersection with the MOFZ near Erzincan, creating a geometry that had some similarity with the modern intersection at Karlıova (Westaway and Arger, 2001). Westaway and Arger (2001) estimated that 29 km of slip occurred on the transform-faulting parts of the MOFZ while it was active. Using the ~13 mm a^{-1} EAFZ slip rate from Westaway (1994), they estimated that the EAFZ became active at ~3 Ma and the MOFZ was active during ~5–3 Ma. Adjusting the EAFZ slip rate to ~8 mm a^{-1} suggests instead that the EAFZ became active at ~4 Ma and the MOFZ became active at ~7–8 Ma and was active until ~4 Ma. This pushes the initiation of the NAFZ back in time from the Early Pliocene (~5 Ma) age preferred by Westaway (1994) and other studies to around the Tortonian–Messinian boundary in the Late Miocene. The implications of this revised age for the NAFZ will be discussed elsewhere.

4. The Turkey–Africa plate boundary

Offshore of southern Turkey, the TR–AF boundary is localised along the Misis–Kyrenia fault zone (e.g., Westaway and Arger, 1996) (Figs. 2 and 12). As Yurtmen et al. (2002) have discussed at length, possible alternative locations farther east, which have been suggested in the literature, do not stand up to careful scrutiny. This discussion is not repeated here. Once onshore, this boundary has been interpreted (e.g., Westaway and Arger, 1996) as splaying into two left-lateral fault zones—the NE-trending Yakapınar–Göksun Fault, which links through to the Sürgü Fault and was the site of the June 1998 Ceyhan earthquake

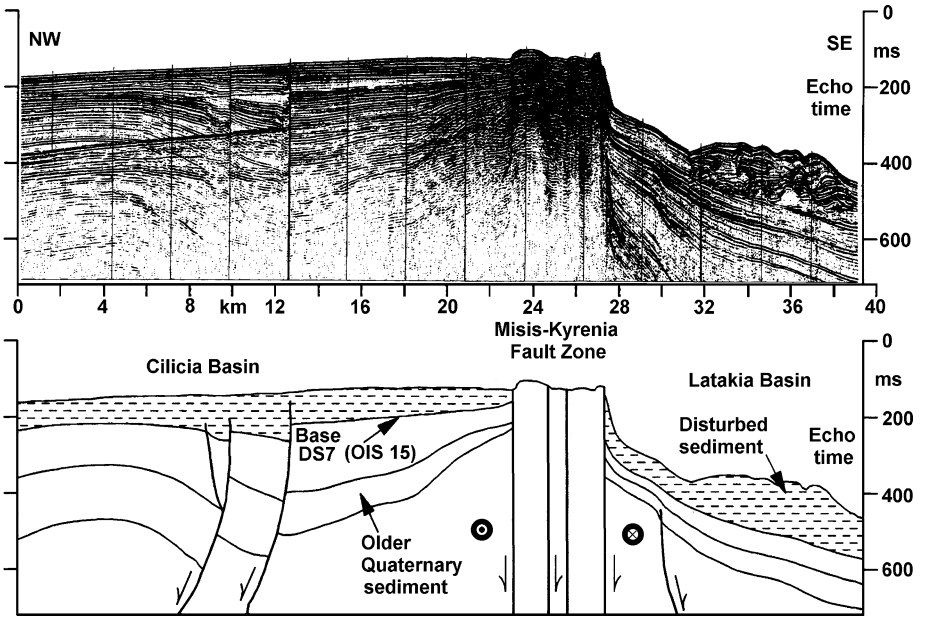

Fig. 12. Seismic reflection record section and interpretation of a profile crossing the Misis–Kyrenia Fault Zone between Karataş and the Kyrenia Range on Cyprus (Fig. 2), adapted from Aksu et al. (1992, Fig. 8). Excluding effects of halokinesis, this is the clearest evidence of active crustal deformation offshore of the Levant coastline, and indicates where the most important offshore active fault zone in this region is located.

(e.g., Aktar et al., 2000); and the ENE-trending Karataş–Osmaniye Fault, which links end-on to the Düziçi Fault in the Amanos Mountains (Fig. 2). Westaway and Arger (1996) suggested that the Karataş–Osmaniye Fault is the more important of the two, with a slip rate of ~5 mm a^{-1}. For much of its length, the line of the Karataş–Osmaniye Fault is obvious in the field; it follows an escarpment up to ~200 m high indicating a small component of relative upthrow of its NW side in addition to the predominant left-lateral slip. The significance of this escarpment was first recognised by McKenzie (1976) using satellite imagery. However, near Osmaniye the line of the Karataş–Osmaniye Fault passes through the Quaternary Ceyhan–Osmaniye volcanic field (e.g., Yurtmen et al., 2000; Arger et al., 2000; Yurtmen and Westaway, 2001a); basalts from volcanic necks such as Toprakkale and Delihalil being found on both sides of this line. Westaway and Arger (1996) thought they had identified the line of the Karataş–Osmaniye Fault along an abrupt scarp edge to the Toprakkale basalt, trending WSW away from this neck. However, this scarp has since been excavated during construction of an irrigation canal, revealing a section through it that establishes it as a river terrace scarp and not a fault scarp (Yurtmen and Westaway, 2001a). Subsequent fieldwork here and farther SW around Delihalil (Yurtmen and Westaway, 2001a) indeed reveals no evidence of any significant left-lateral offset along this fault line since the youngest basalt-dated to ~0.4 Ma (Arger et al., 2000) was erupted. It thus now seems clear that the Karataş–Osmaniye Fault is not active at present (contra Westaway and Arger, 1996), although it clearly was important at an earlier stage.

Evidence in support of this point of view is also provided by the GPS data (McClusky et al., 2000), which report motions of three points situated between the DSFZ and the Karataş–Osmaniye Fault: SENK (Şenköy), ULUC (Uluçınar), and DORT (Dörtyol) (Fig. 10a). Relative to SENK, ULUC is moving northward at 1.1 ± 2.1 mm a^{-1} and westward at 6.1 ± 2.3 mm a^{-1}; DORT is moving relative to SENK at 0.7 ± 2.0 mm a^{-1} northward and 5.7 ± 2.1 mm a^{-1} westward (McClusky et al., 2000), As McClusky et al. (2000) noted, SENK is thus moving roughly as expected for a point within the stable interior of the African plate, but the state of motion of ULUC and DORT, farther northwest, is much closer to what is expected for points within the Turkish plate. Their motion is indeed roughly ~2 mm a^{-1} ~NE relative to the interior of this plate, rather than the ~8–9 mm a^{-1} towards the east that is expected between the stable interiors of these plates (Fig. 11d and e). These GPS results have two main implications. First, there is significant relative motion between SENK and ULUC and DORT, which must involve distributed deformation across the southern part of the Amanos Mountains, as no major fault is present. Second, the overall left-lateral slip rate across the Karataş–Osmaniye and Yakapınar–Göksun faults is ~2 mm a^{-1}. Since the slip rate on the former is now assumed to be zero, the slip rate on the latter can thus be estimated as ~2 mm a^{-1}. This interpretation is consistent with the GPS point KDRL (Kadirli), located between the Karataş–Osmaniye and Yakapınar–Göksun faults, which has negligible motion relative to ULUC and DORT. This estimated left-lateral slip rate of ~2 mm a^{-1} on the Yakapınar–Göksun Fault also matches well the predicted ~1.9 mm a^{-1} left-lateral slip rate on the Sürgü Fault and ~2.3 mm a^{-1} rate of relative motion across it, given its transpressive geometry (Fig. 11c).

Fig. 11d shows relative motion vectors calculated at Delihalil on the Karataş–Osmaniye Fault, along with the vectors deduced earlier (Fig. 11c) for points on the western side of the Amanos Fault at the eastern margin of the Amanos Mountains. This solution is derived assuming the same kinematic model as before, plus a 2-mm a^{-1} left-lateral slip rate towards the NE on the Yakapınar–Göksun Fault with no slip on the Karataş–Osmaniye Fault. Vector triangle closure indicates that this point is moving westward relative to the stable interior of the African plate at ~7 mm a^{-1}, roughly consistent with the GPS observations at ULUC and DORT. It indicates that the predicted motion of points on the eastern margin of the Amanos Mountains (denoted by reference frame t2) relative to TR and AR is subparallel to the TR–AR motion. No major component of shortening is thus required across the Amanos Mountains, the geometry tentatively indicating minor distributed WNW–ESE extension, superimposed on the a important component of left-lateral distributed simple shear, which is indicated by the SSW predicted motion of the reference frame AF^{+} (containing points between the western margin of the Amanos Mountains and the Yakapınar–Göksun Fault) and t2. It is thus tentatively predicted that the ~9 mm

a^{-1} of overall SSW–NNE relative motion between TR and AR is partitioned as ~2 mm a^{-1} of localised left-lateral slip on the Yakapınar–Göksun Fault, ~3.5 mm a^{-1} of distributed left-lateral SSW–NNE simple shear across the Amanos Mountains, and ~3.5 mm a^{-1} of localised slip on SSW–NNE trending faults east of the Amanos Mountains (i.e., on the Amanos and East Hatay faults).

Following Westaway and Arger (1996), it is presumed that the Karataş–Osmaniye Fault and its end-on continuation into the Amanos Mountains, the Düziçi Fault, became active around the time (now estimated at ~7 Ma) when the Turkish plate first came into being with the initiation of the MOFZ. As these faults remain subparallel to the TR–AR and TR–AF^+ relative motions, slip on them would obviate the need for the component of distributed left-lateral simple shear within the Amanos Mountains that has been deduced. A possible explanation for this feature can be proposed, given that the Karataş–Osmaniye Fault cuts across the suture of the former southern branch of the Neotethys Ocean (Westaway and Arger, 1996), passing through the ophiolite that has been obducted along this suture. It can be presumed that within such ophiolite the base of the brittle layer will be deeper than elsewhere, due to the mafic rheology. As a result of the high normal stress across the deeper part of such a fault, a high shear stress would be required to overcome friction to enable such a fault to slip. As the TR–AF* or TR-y motion is oblique to the ~N60°E strike of the Karataş–Osmaniye Fault, this fault can be presumed to have initially had a transpressive slip sense. As a result of the increasing compression across it, it can thus be presumed that a point was eventually reached when it was mechanically "easier" for slip on it to cease and for the relative plate motion to migrate elsewhere. Supporting evidence for this view is provided by analysis of the Ceyhan earthquake of 27 June 1998 (M_w 6.2), which occurred near the southern end of the Yakapınar–Göksun Fault. This event and its aftershocks occurred at the depth range of ~20–40 km (Aktar et al., 2000), indicating brittle behaviour at an unusually great depth.

The proposed regional kinematic model suggests that the modern strike-slip boundary forming the eastern margin of the Turkish plate is in almost all localities optimally oriented subparallel to the local plate motions. The NAFZ is likewise a good approximation to a transform fault zone, oriented subparallel to the relative motion across it (e.g., Westaway, 1994; McClusky et al., 2000). The main exception is in the vicinity of İskenderun Gulf. In this vicinity, it has been suggested that the Karataş–Osmaniye Fault, which is optimally oriented, has become locked, requiring a combination of distributed deformation and slip on the Yakapınar–Göksun Fault farther north. It has been suggested that this difficulty results from the presence within the plate boundary zone of ophiolitic crust that has relatively high strength. The presence of this localised patch of high-strength crust thus appears to have increased the normal stress across the Karataş–Osmaniye Fault, preventing continued slip on it.

The tentative age estimate of ~2 Ma made earlier for the Sürgü Fault implies the same age for the Yakapınar–Göksun Fault, suggesting that the Karataş–Osmaniye Fault ceased to be active at that time. It is thus suggested that, between ~4 and ~2 Ma, a throughgoing left-lateral fault zone existed across the Amanos Mountains, linking the Karataş–Osmaniye Fault end on into the Düziçi Fault. This in turn linked end-on into the Gölbaşı–Türkoğlu Fault, presumably with a splay onto the Amanos Fault at Türkoğlu. As Westaway and Arger (1996) pointed out, restoring this geometry of slip would juxtapose the southern end of the Doluca Fault (Fig. 2) against the northern end of the Amanos Fault. It is thus presumed that, before the Gölbaşı–Türkoğlu Fault developed at ~4 Ma, throughgoing left-lateral faulting already cut through the Amanos Mountains, with the Doluca Fault—not the Gölbaşı–Türkoğlu Fault—forming the end-on continuation of the left-lateral slip on the Düziçi Fault as well as the Amanos Fault. This geometry is illustrated in Westaway and Arger (1996, Fig. 9c), although it is now presumed to have existed between ~7 and ~4 Ma, rather than the ~5- to ~3-Ma timing suggested in that study. As Westaway and Arger (1996) also pointed out, it can be presumed that during this phase of deformation the component of TR–AR motion accommodated on the Doluca Fault stepped to the right in the vicinity of Kahraman Maraş—across a zone of crustal shortening—onto the southern end of the MOFZ (Fig. 1). However, the present study indicates that the Neo-

gene–Quaternary history of faulting and crustal deformation in and around the Amanos Mountains has been rather more complex than Westaway and Arger (1996) proposed. As well as the additional complexity of major faulting identified in this study, it is now also predicted that the overall shape of this region has changed substantially on this time scale due to the components of distributed crustal deformation that are required, which this earlier work did not consider.

5. Summary and discussion

To illustrate the main consequences of the proposed kinematic model, Fig. 13 illustrates predicted northward variations in slip rate along the DSFZ, between the Tiran Strait (at the southern end of the Gulf of Aqaba; Fig. 1) and Türkoğlu at the northern end of the Amanos Fault (Fig. 2). At each point, V is the rate of relative motion between the African and Arabian plates, calculated using spherical trigonometry (including the effect of Earth ellipticity) from the position of the point relative to the assumed Euler pole at 31.1°N 26.7°E, given the assumed rate of relative rotation. α is the observed strike of the principal DSFZ strand, θ is the difference in angle between α and the tangential direction to the Euler pole, and U is the maximum possible rate of left-lateral slip on this fault strand, calculated using Eq. (1). Solutions illustrated are for rates of relative rotation of 0.385° Ma^{-1} (a) and 0.42° Ma^{-1} (b). In (a), the rate of relative plate motion increases from ~5.5 mm a^{-1} in the south to ~7.8 mm a^{-1} in the north. However, its component parallel to the observed strike-slip faulting varies rather differently. In the south, the two rates—V and U—are indistinguishable, as the plate boundary is—to a good approximation—a series of transform fault segments. However, from Lebanon northward the two rates diverge, as the observed faulting follows a series of transpressive stepovers, those in Lebanon and southern Turkey being more severely misaligned relative to the plate motion than in Syria. The maximum predicted rate of left-lateral strike-slip faulting is thus not in southern Turkey but in Syria, and is ~6.1–6.2 mm a^{-1}. In (b), for 0.42° Ma^{-1}, the rates of relative plate motion increase northward in proportion, from ~6.0 mm a^{-1} to ~8.7 mm a^{-1}, the peak rate of left-lateral faulting being ~6.7 mm a^{-1}, again in Syria. Solution (a) is constrained to roughly match Meghraoui's (2002) archaeological evidence for the slip rate on the Masyaf Fault if the age of the observed offset is 210 BC. Solution (b) is constrained to roughly match the higher estimate if this offset first developed in the earthquake in 63 BC; the ~6-mm a^{-1} slip rate that it requires on the southern DSFZ is also about the maximum value that is tenable given the local evidence (e.g., Klinger et al., 2000). Taking these constraints into account, the rate of AF–AR relative rotation is assigned a nominal value of 0.40° Ma^{-1}, with a margin of uncertainty of $\pm$0.02° Ma^{-1}.

Except for the southernmost part of the Lebanon stepover, it is noteworthy that along all three stepovers the geometry is such that a constant predicted rate of strike-slip is maintained, although the northern end of the stepover is substantially farther from the Euler pole than the southern end. This is possible because at its northern end each stepover is more severely misaligned than at its southern end. Thus, in terms of the notation in Eq. (1), for each stepover, V and θ both increase northward in such a manner that $U=V\cos(\theta)$ remains virtually constant.

The greatest complexity is observed around the southern end of the Lebanon stepover, where θ increases gradually from ~6° in the Hula Basin to ~48° in the central part of the Lebanon stepover, as α increases from −7° (i.e., 353°) to 30°. The overall value of U deduced for this region can be presumed to reflect the combined slip rates on the Roum fault and the southern parts of the Yammouneh and Serghaya faults. The predicted northward tapering in U is thus presumed to reflect a northward decrease in the slip rate along the Roum Fault, which splays from the Yammouneh Fault in the vicinity of the Hula Basin. Farther north, the slip on the Roum Fault is presumed (after Griffiths et al., 2000) to gradually die out into the distributed deformation within the southern Lebanon Mountains. The small difference between the observational estimate of the slip rate on the southern Yammouneh Fault and the plateau value of U farther north is assumed to indicate the slip rate on the southern part of the Serghaya Fault. Farther north, this small component of slip is presumed to be transferred leftward onto the northern part of the Yammouneh Fault, as the Serghaya Fault shows no

evidence for active slip in the vicinity of the Syria–Lebanon border south of Homs (see Fig. 5 and earlier discussion).

In the northern part of the study region, multiple en echelon left-lateral faults are also present, all typically oriented SSW–NNE (Fig. 11b). It is evident that this

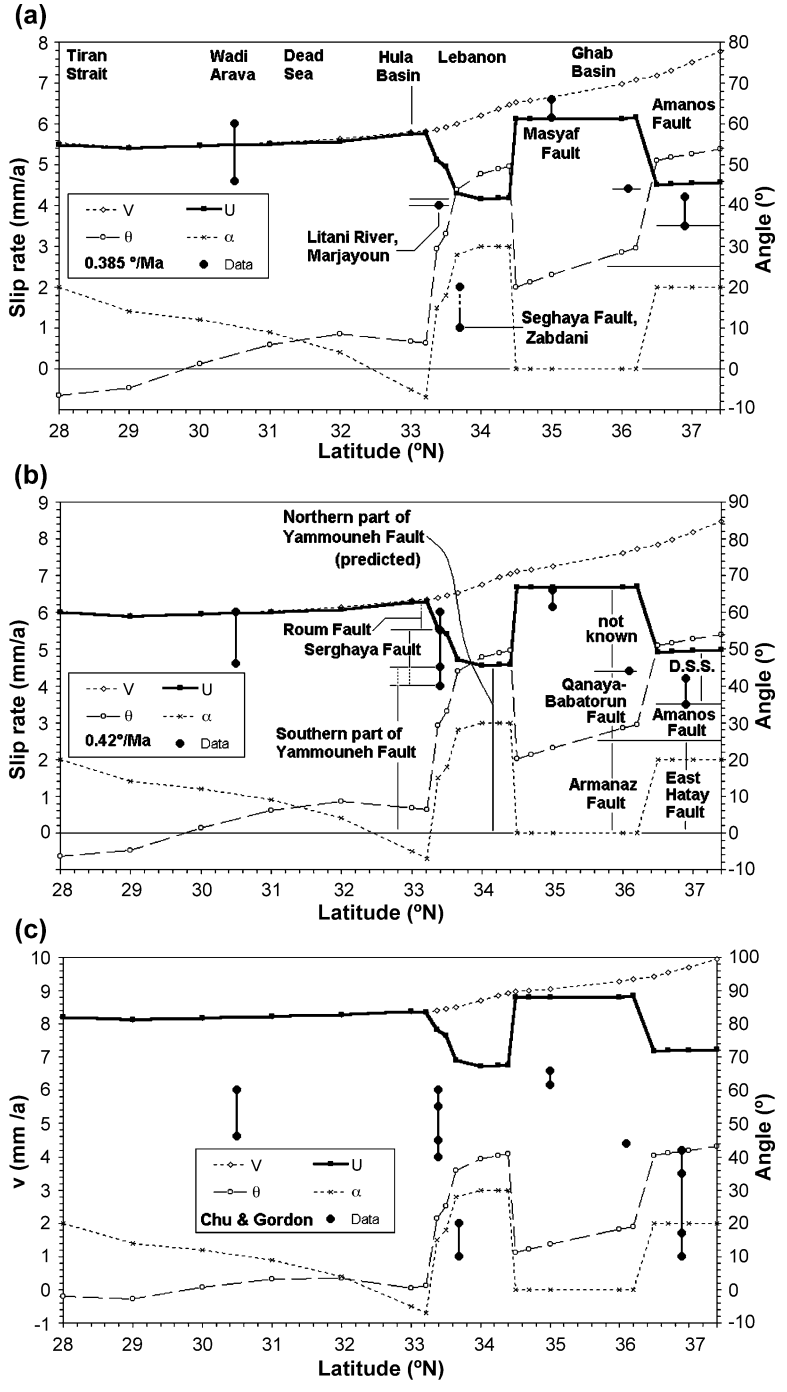

geometry manages to avoid as much as possible the requirement for any faulting in regions of high-strength crust, notably between Cyprus and the Levant coastline, where the deep (~2 km) bathymetry (e.g., Kempler and Garfunkel, 1994; Vidal et al., 2000) indicates that the weak lower-crustal layer is likely to be thin, causing the crust to be strong (e.g., Westaway, 2002c,d). Faulting also manages to avoid as much as possible the vicinity of the Neotethys suture, where mafic material at depth can also be expected, likewise causing high strength in the crust. Faulting does occur in the vicinity of this suture at the southern end of the Yakapınar–Göksun Fault, and transects this suture at the Çelikhan stepover. However, between these localities it keeps well away from this suture, with the Yakapınar–Göksun and Sürgü Faults north of it and the other faulting on its southern side (Fig. 10b). This geometry presumably allows these faults to be located in regions of weaker crust that has been easier to fracture.

The observed regional deformation sense raises a semantic difficulty, concerning where the notional AF–AR–TR "triple junction" is located. It is evident from preceding discussion that no point onshore in Turkey, with the possible exception of the extreme southern part of Hatay Province around the Şenköy GPS point, can be regarded as within the stable interior of the African Plate. The strike-slip faulting in the extreme south of Turkey can instead be regarded as forming a distributed "boundary zone" between the Turkish and Arabian plates, across which the estimated ~8.7 mm a^{-1} of left-lateral motion has tentatively been shown to be accommodated by localised left-lateral slip at ~2 mm a^{-1} on the Yakapınar–Göksun Fault, ~1 mm a^{-1} on the Amanos Fault, and ~2.5 mm a^{-1} on the East Hatay Fault, plus subparallel distributed left-lateral simple shear at ~3.2 mm a^{-1} across the Amanos Mountains. This faulting is oriented subparallel to the predicted TR–AR motion, with no simple relationship to the sense of motion of the African plate relative to either of the other plates, and its kinematics are also not sensitive to changes in the state of motion of the African plate (as is illustrated by comparing Fig. 11d and e). Thus, it seems to make no sense to regard any of this zone as part of the African Plate. However, no localised triple

Fig. 13. Summaries of the geometry of the Dead Sea Fault Zone, between the Tiran Strait and Türkoğlu at the northern end of the Amanos Fault. At each point, V is the rate of relative motion between the African and Arabian plates, calculated using spherical trigonometry (including the effect of Earth ellipticity) from the position of the point relative to the assumed Euler pole at 31.1°N 26.7°E, given the assumed rate of relative rotation. α is the observed strike of the principal DSFZ strand, measured clockwise from north. θ is the difference in angle between α and the tangential direction to the Euler pole. U is the maximum possible rate of left-lateral slip on this fault strand, calculated using Eq. (1), as $V\times\cos(\theta)$. Solutions illustrated are for rates of relative rotation of 0.385° Ma^{-1} (a) and 0.42 ° Ma^{-1} (b). Solution (c) is for alternative Euler vector (pole: 31.5°N 23.0°E; rotation rate: 0.403° Ma^{-1}) determined by Chu and Gordon (1998) from analysis of the Red Sea oceanic spreading centre. Data comprise, (1) for the Arava Fault, the range of slip rate estimates from Zhang (1998), of 39 m/8.5 ka=4.6 mm a^{-1}, and Ginat et al. (1998), of ~15 km/~2.5 Ma=6 mm a^{-1}. (2) In southern Lebanon, the offset of the Litani River gorge by the southern Yammouneh Fault (see main text) suggests a slip rate of ~3.5 km/870 ka=4.0 mm a^{-1}. The southern Serghaya Fault has an estimated Holocene slip rate of ~1–2 mm a^{-1} (Gomez et al., 2001a,b). The southern Roum Fault has an estimated slip rate of ~0.5 mm a^{-1} (see main text). (3) Estimates from trenching (Meghraoui, 2002) at El Harif near Masyaf, of 13.6 m/2212 a=6.15 mm a^{-1}, and 13.6 m/2065 a=6.6 mm a^{-1}. (4) Estimates of the Quaternary slip rate on the Amanos Fault, of 1.0–1.7 mm a^{-1}, from Yurtmen et al. (2002), added to the estimate for the East Hatay Fault of ~10 km/~4 Ma=~2.5 mm a^{-1} (see main text). (5) The sum of the slip rate estimates for the Qanaya–Babatorun Fault, ~10 km/~5.3 Ma=~1.9 mm a^{-1}, and ~2.5 mm a^{-1} for the Armanaz Fault, based on the assumption that it is an end-on continuation of the East Hatay Fault and so has the same slip rate. In localities where there is significant partitioning of the relative plate motion, labelling indicates estimates of how it is subdivided. In southern Lebanon, it is assumed that the northward tapering in U reflects the observed northward decrease from ~0.5 mm a^{-1} in the slip rate along the Roum Fault as its slip gradually dies out into the distributed deformation within the southern Lebanon Mountains, plus lateral variations with up to ~1–1.5 mm a^{-1} of slip on the Serghaya Fault and ~4–4.5 mm a^{-1} of slip on the Yammouneh Fault (as illustrated in part b). In contrast, in northern Lebanon, the only significant slip seems to be on the northern Yammouneh Fault, which appears to take up all the slip on the Masyaf Fault with a change in geometry, and is thus predicted to be slipping at [~6–6.5 mm a^{-1}]×cos(50°)/cos(20°) or ~4–4.5 mm a^{-1}. Thus, the slip rate may remain roughly constant throughout the length of the Yammouneh Fault. In southern Turkey, the preferred estimate for the combined slip rate on the Amanos and East Hatay Faults is ~3.5 mm^{-1}, the excess of U over this figure being tentatively assumed to be accommodated by a component of distributed left-lateral simple shear (D.S.S.) across the Amanos Mountains. As an alternative, it could instead be accommodated by faster (by up to ~0.7 mm a^{-1}) slip on the Amanos Fault, faster slip on the East Hatay Fault, or up to ~1.8 mm a^{-1} of slip to the east of the East Hatay Fault. In northern Syria, the mismatch between the reported data and the predicted values of U (labelled "not known") could indicate the sum of the slip rates on the other fault strands in this vicinity, such as a ~1.8 mm a^{-1} slip rate on the Afrin Fault, or it may indicate a component of fault-parallel distributed simple shear, like in the Amanos Mountains, or a combination of the two.

junction can be identified. Moving northward from southern Hatay, the state of motion appears instead to change gradually away from what is expected for the stable interior of the African plate to what is predicted for points within this deforming plate boundary zone.

The Klinger et al. (2000) Euler pole that has been used to predict the DSFZ slip sense (Fig. 1) is based on Late Pleistocene and Holocene slip sense indicators, thus facilitating comparison with the other field and geodetic evidence discussed, which represents comparable time scales. Positions of other published AR–AF poles differ from it by hundreds of kilometres. For instance, the NUVEL-1A pole based on global plate circuit closure (DeMets et al., 1994) is located ~800 km farther SSW, and predicts strongly transpressive relative motion across the southern DSFZ (Klinger et al., 2000) indicating that it is mislocated. In an attempt to obtain a more satisfactory fit, Chu and Gordon (1998) determined a new pole at 31.5°N 23.0 °E (ω 0.403° Ma^{-1}) based on analysis of the Red Sea oceanic spreading centre. This pole is ~350 km west of the Klinger et al. (2000) pole (Fig. 1). Being farther from the DSFZ, it predicts less dramatic lateral variations in slip sense along it. However, it does require transform faulting along the southern DSFZ and transpression farther north (Fig. 13c), although the predicted ratio of shortening to left-lateral slip is everywhere less than for the Klinger et al. (2000) pole. Nonetheless, predicted rates of relative plate motion for the Chu and Gordon (1998) Euler vector are faster everywhere along the DSFZ (Fig. 13c), the predicted rates of left-lateral slip being ~8 mm a^{-1} in the south compared with ~5.5–6 mm a^{-1} (a mismatch of ~40%), and ~7 mm a^{-1} in the north compared with ~4.5–5 mm a^{-1} (a mismatch of ~50%). Thus, its predictions overestimate all observational evidence for the slip rate throughout this fault zone.

Chu and Gordon (1998) suggested that actual DSFZ slip rates will be less than the predictions from their AR–AF Euler vector, due to extension across the Gulf of Suez (Fig. 1). Bosworth and Taviani (1996) estimated the rate of this extension as ~0.8–1.2 mm a^{-1}. However, this estimate is derived from uplift rates of marine terraces, combined with the assumption that coastlines are uplifting in footwalls of active normal faults, together with more assumptions about ratios of footwall uplift to hanging-wall subsidence that are now considered questionable (see, e.g., Westaway, 2002c). This uplift may well instead be caused, at least in part, by coupling between surface processes and lower-crustal flow, which is very widespread (e.g., Westaway, 2002a,b) and has frequently been mistaken for effects of active faulting when observed in and around the Mediterranean region (e.g., Arger et al., 2000; Westaway et al., 2003). However, even if Bosworth and Taviani (1996) are correct, this extension would be too slow to account for the mismatch between the observed and predicted DSFZ slip rates in Fig. 13c.

A possible reason for this discrepancy using the Chu and Gordon (1998) Euler vector is that the instantaneous Euler vector has adjusted over time, so observations of the Red Sea spreading centre indicate its time-averaged position over a longer time scale than observations of Late Quaternary faulting. Ten Brink et al. (1999) have indeed noted abundant evidence of small changes in the sense of slip along the southern DSFZ during its evolution, consistent a sequence of adjustments to the position of this pole. However, incorporating such fine detail into a kinematic model for the whole of the Middle East and eastern Mediterranean region is beyond the scope of this study. An additional possibility also springs to mind when the typical quality of fit between observed and predicted Red Sea magnetic spreading anomalies in Chu and Gordon (1998) is inspected; that this quality of fit may be nonunique, and the overall fit may not be significantly worse if calculated for the alternative Euler vector deduced by Klinger et al. (2000) or in this study. However, testing this possibility is also beyond the scope of this study.

A number of uncertainties remain in the kinematics of this study region. First, as already noted, in northern Syria, both the detailed present-day partitioning of the AF–AR relative motion and the age and slip history of each of the left-lateral fault systems remain unclear. As Fig. 13 indicates, the present scheme indeed cannot account for ~1.5–2 mm a^{-1} of the ~6–6.5 mm a^{-1} of left-lateral slip that is estimated to be occurring in this region. Furthermore, the ~17 km measurement of the total slip linking through to the SSW from the Gölbaşı area (from Westaway and Arger, 1996) exceeds the ~10 km of slip estimated on the East Hatay Fault, its presumed SSW continuation.

It remains unclear at this stage how to resolve this discrepancy. Possible explanations include, first, that ~7 km of left-lateral slip passes southward from the Gölbaşı area onto other faults east of the East Hatay Fault, possibly being taken up on the Kırkpınar Fault and then accommodated farther south on the Afrin Fault in northern Syria (Fig. 2). Second, the ~10-km estimate of the total slip on the East Hatay Fault (Fig. 3) depends on piercing points on its western side in Turkey and on its eastern side in Syria. Possible inconsistencies between the mapping in the two countries may mean that this estimate is wrong, and it may underestimate the true amount of slip on this fault. Adding this extra ~7 km/~4 Ma or ~1.8 mm a^{-1} component of N20°E relative motion would mean that the state of motion of points on the western side of the Amanos Fault would lie to the SSW of reference frame AF* and very close to AF^{+} in Fig. 11d and e, thus removing much (or possibly, even, all) of the requirement for distributed left-lateral simple shear across the Amanos Mountains. It would also increase the "observed" rate of left-lateral slip across northern Syria from ~4.4 to ~6.2 mm a^{-1}, virtually eliminating any mismatch relative to the model predictions (Fig. 13). However, the equivalent adjustment to the vector polygon for Türkoğlu (Fig. 11c) would adversely affect the local solution. It would require the state of motion of the reference frame for points south of the Gölbaşı–Türkoğlu Fault to be adjusted from t1 to somewhere close to AF* in the figure. This would remove the kinematic consistency already deduced with regard to the Sürgü Fault, as it would predict left-lateral transtension (not transpression), unless the slip sense or rate on the Gölbaşı–Türkoğlu Fault was also adjusted. One could suggest, for instance, that its slip rate may be higher. After allowing for the inherent difficulties in measuring river gorge offsets (see, e.g., Yurtmen et al., 2002), the post-OIS 22 offsets along this fault could be, say, 4 km, not ~3.5 km. If so, the slip rate has been ~4.6, not ~4 mm a^{-1}, predicting ~18, not ~16, km, of slip since ~4 Ma, and requiring ~15, not ~17, km of slip to pass SSW from the Gölbaşı area—at a rate of ~3.8, not ~4.3, mm a^{-1}. Both these adjustments would act to restore kinematic consistency in Fig. 11c, as would adjusting the slip sense assumed for the Gölbaşı–Türkoğlu Fault from N65°E (appropriate for its western end near Türkoğlu) to ~N75°E (appropriate for its central part).

GPS (e.g., McClusky et al., 2000) now also allows the partitioning of slip across the various strands of the northern DSFZ to be investigated. Ground control point SAKZ (Sakçagöz) is located near the northern edge of the limestone uplands just east of the northernmost Karasu Valley. It is thus probably north of any fault segment running through these uplands linking the East Hatay Fault with the Kırkpınar Fault or the EAFZ near Gölbaşı (Figs. 2 and 10a). Point GAZI (Gaziantep) is east of all known strands of the DSFZ in southern Turkey. Point DORT (Dörtyol, already discussed), west of the Amanos Mountains, is assumed to be located within the AF^{+}reference frame (Fig. 11d and e). The GAZI-DORT relative motion thus provides an observational test of the AR–AF^{+}prediction in Fig. 11d and e. It is determined (from McClusky et al., 2000) as 3.7±1.8 mm a^{-1} northward and 2.6±1.9 mm a^{-1} eastward, or ~4.5±2.6 mm a^{-1} towards the ~NNE. The SAKZ-DORT relative motion is determined (from McClusky et al., 2000) as 1.7±2.0 mm a^{-1} northward and 1.3±2.1 mm a^{-1} eastward, or ~2.4±2.6 mm a^{-1} towards the ~NNE. The GAZI-SAKZ relative motion is likewise determined as 2.0±1.8 mm a^{-1} northward and 1.3±1.9 mm a^{-1} eastward, or ~2.4±2.6 mm a^{-1} towards the ~NNE.

The GAZI-DORT estimate thus falls within 1σ of the ~6.7 mm a^{-1} prediction of the AR–AF^{+}relative motion in Fig. 11, indicating consistency. The GAZI-SAKZ relative velocity provides an estimate of the combined slip rate on the East Hatay Fault and any other en echelon fault strands farther east, estimated earlier as within the range ~2.5–4.3 mm a^{-1}. This whole range of values falls within 1σ of the GPS estimate. The SAKZ-DORT relative velocity provides an estimate of the sum of the slip rate on the Amanos Fault plus the rate of any distributed left-lateral simple shear across the Amanos Mountains. Earlier discussion indicated that this relative motion could be predicted to lie between ~1.0 mm a^{-1} (the lower bound to the slip rate on the Amanos Fault plus no simple shear) and ~5 mm a^{-1} (the ~1.7 mm a^{-1} upper bound to the slip rate on the Amanos Fault plus ~3.2 mm a^{-1} of simple shear). Again, this whole range of values falls within 1σ of the GPS estimate. It is thus evident that the GPS evidence is consistent with the range of kinematic models suggested in this study, but it is not yet sufficiently tightly constrained to eliminate any of the possible range of alternatives.

6. Conclusions

A revised kinematic model has been determined for the Dead Sea Fault Zone and the left-lateral fault zones in southeastern Turkey. The relative motions of the African and Arabian plates across the DSFZ are represented by relative rotation about an Euler pole at 31.1°N 26.7°E, at a rate that is estimated as $0.40\pm0.02^{\circ}$ Ma^{-1}. The northern DSFZ, in Syria and southern Turkey, is regarded as a series of transpressional stepovers, along which the left-lateral slip is substantially slower than the relative plate motion, because this slip is strongly oblique to the relative plate motion. The revised slip rate on the EAFZ is estimated as ~8 mm a^{-1}. At this rate, restoring the observed slip requires the age of the EAFZ to be ~4 Ma. The previous phase of deformation (Westaway and Arger, 2001), which involved slip on the MOFZ before the EAFZ came into being, is thus dated to ~7–4 Ma, suggesting initiation of the NAFZ at ~7 Ma, not ~5 Ma as has previously been thought.

The predicted rate of relative motion between the stable interiors of the Turkish and African plates in the vicinity of their common boundary onshore of İskenderun Gulf is estimated as ~9 mm a^{-1} towards S81°W (Fig. 11d and e). However, the "promontory" of the African plate adjacent to this boundary is moving westward relative to the stable interior of this plate at ~8 mm a^{-1}. The rate of localised left-lateral slip on the onshore part of this boundary, the NE-trending Yakapınar–Göksun Fault, is thus estimated as only ~2 mm a^{-1}. This locality can also be regarded as within a distributed boundary zone between the Turkish and Arabian plates. The estimated TR–AR relative motion is at ~8.7 mm a^{-1} towards the SSW, partitioned with ~2 mm a^{-1} of localised left-lateral slip on the Yakapınar–Göksun Fault, and at least ~3.5 mm a^{-1} of localised left-lateral slip on the Amanos Fault and East Hatay Fault, with at most ~3.2 mm a^{-1} of distributed left-lateral simple shear across the Amanos Mountains in between. However, the combined slip on left-lateral faults east of the Amanos Mountains may be as high as ~6 mm a^{-1}, with slip at ~1.7 mm a^{-1} on the Amanos Fault and at ~4.3 mm a^{-1} on the East Hatay Fault and any active faults farther east. This requires no more than ~0.7 mm a^{-1} of distributed simple shear across the Amanos Mountains, raising the possibility that this component of deformation may in fact be zero, this small nonzero value possibly indicating a closure error arising from minor errors in predicted values of other relative motion vectors. It is proposed that this TR–AF plate boundary first developed at the same time as the NAFZ, but its original geometry involving left-lateral slip on the Karataş–Osmaniye Fault has since become locked by the presence of relatively strong ophiolitic crust within this fault zone.

The total left-lateral slip on the northern DSFZ in southern Turkey is estimated as at least ~65 km, partitioned with ~45 km on the Amanos Fault, ~10 km on the East Hatay Fault, and a further ~10 km on the Kırkpınar Fault farther east. Much of this slip is inferred to have occurred during the Miocene, before the modern geometry of this plate boundary zone developed. When it first formed, the AF–AR plate boundary was relatively complex. That is, it appears to have initially reactivated preexisting structures in the Palmyra foldbelt and in the Gaziantep region of southern Turkey, which were significantly misaligned relative to the plate motion, requiring major components of shortening as well as left-lateral slip. The transition from this initial geometry to the present localised geometry of the DSFZ across western Syria occurred within the Miocene.

This quantitative kinematic model—which is consistent with the available structural and geodetic evidence—thus demonstrates, for the first time, how it is possible for the left-lateral faulting accommodating the NNW–SSE relative motion between the Arabian and African plates in NW Syria to "dovetail" into the left-lateral faulting accommodating the WSW–ENE relative motion between the Turkish and Arabian plates in SE Turkey.

Acknowledgements

I would like to thank the many people who have collaborated with me in the field in the present study region, or have provided technical or logistical support or stimulating discussions, during this programme of research that began in southeastern Turkey in 1990 and in Syria in 2001. I particularly thank Jan Arger, Erdin Bozkurt, David Bridgland, Maryam Bshesh, Tuncer Demir, John Mitchell, Graham Philip, Saadettin Tonbul, and Sema Yurtmen. Mustapha

Meghraoui kindly provided a preprint, and I am also grateful to Francisco Gomez and Paul Meijer for thoughtful and constructive reviews.

References

Aksu, A.E., Calon, T.J., Piper, D.J.W., Turgut, S., Izdar, E., 1992. Architecture of late orogenic Quaternary basins in northeastern Mediterranean Sea. Tectonophysics 210, 191–213.

Aktar, M., Ergin, M., Özalaybey, S., Tapırdamaz, C., Yörük, A., Biçmen, F., 2000. A lower-crustal event in the northeastern Mediterranean: the 1998 Adana earthquake (M_w=6.2) and its aftershocks. Geophys. Res. Lett. 27, 2361–2364.

Ambraseys, N.N., Barazangi, M., 1989. The 1759 earthquake in the Bekaa Valley: implications for earthquake hazard assessment in the eastern Mediterranean region. J. Geophys. Res. 94, 4007–4013.

Arger, J., Mitchell, J., Westaway, R., 2000. Neogene and Quaternary volcanism of south-eastern Turkey. In: Bozkurt, E., Winchester, J.A., Piper, J.D.A. (Eds.), Tectonics and Magmatism of Turkey and the Surrounding Area, Spec. Publ.-Geol. Soc. London, vol. 173, pp. 459–487.

Armijo, R., Meyer, B., Hubert, A., Barka, A., 1999. Westward propagation of the North Anatolian fault into the northern Aegean: timing and kinematics. Geology 27, 267–270.

Arpat, E., Şaroğlu, F., 1972. The East Anatolian fault system: thoughts on its development. MTA Bull. 78, 33–39.

Atan., O. 1969. Eğribucak-Karacören (Hassa)-Ceylânlı-Dazevleri (Kırıkhan) arasındaki Amanos Dağlarının Jeolojisi. Report no. 139, General Directorate of Mineral Research and Exploration, Ankara, 85 pp.

Ben-Menahem, Z., 1981. Variation of slip and creep along the Levant Rift over the past 4500 years. Tectonophysics 80, 183–197.

Besançon, J., Sanlaville, P., 1993. La vallée de l'Oronte entre Rastane et Aacharné. In: Sanlaville, P., Besançon, J., Copeland, L., Muhesen, S. (Eds.), Le Paléolithique de la Vallée Moyenne de L'Oronte (Syrie): Peuplement et Environnement, Brit. Archaeol. Rev., Int. Ser., vol. 587, pp. 13–39.

Bosworth, W., Taviani, M., 1996. Late Quaternary reorientation of stress field and extension direction in the southern Gulf of Suez: evidence from uplifted coral terraces, mesoscopic fault arrays, and borehole breakouts. Tectonics 15, 791–802.

Bourcart, J., 1940. Recherches stratigraphiques sur le Pliocène et le Quaternaire du Levant. Bull. Soc. Geol. Fr. 10 (5), 207–230.

Brew, G., Lupa, J., Barazangi, M., Sawaf, T., Al-Imam, A., Zaza, T., 2001. Structure and tectonic development of the Ghab basin and the Dead Sea fault system, Syria. J. Geol. Soc. (Lond.) 158, 665–674.

Bridgland, D.R., Philip, G., Westaway, R., White, M., 2003. A long Quaternary terrace sequence in the valley of the River Orontes, near Homs, Syria. Curr. Sci. 84, 1080–1089.

Butler, R.W.H., Spencer, S., 1999. Landscape evolution and the preservation of tectonic landforms along the northern Yammouneh Fault, Lebanon. In: Smith, B.J., Whalley, W.B., Warke, P.A. (Eds.), Uplift, Erosion, and Stability: Perspectives on Long-term Landscape Development, Spec. Publ.-Geol. Soc. London, vol. 162, pp. 143–156.

Butler, R.W.H., Spencer, S., Griffiths, H.M., 1997. Transcurrent fault activity on the Dead Sea Transform in Lebanon and its implications for plate tectonics and seismic hazard. J. Geol. Soc. (Lond.) 153, 757–760.

Butler, R.W.H., Griffiths, H.M., Spencer, S., 1998. The structural response to evolving plate kinematics during transpression; evolution of the Lebanese restraining bend of the Dead Sea Transform. In: Holdsworth, R.E., Strachan, R.A., Dewey, J.F. (Eds.), Continental Transpressional and Transtensional Tectonics, Spec. Publ.-Geol. Soc. London, vol. 135, pp. 81–106.

Çetin, H. 2000. Paleoseismology of the Ecemiş Fault: mid results. In: Workshop on Active Tectonics of Western Turkey, in Memoriam to Paul L. Hancock, İstanbul Technical University, June 2000, Abstract and Programme Volume, pp. 47–55.

Chaimov, T.A., Barazangi, M., Al-Saad, D., Sawaf, T., Gebran, A., 1990. Crustal shortening in the Palmyride fold belt, Syria, and implications for movement along the Dead Sea fault system. Tectonics 9, 1369–1386.

Chu, Dezhi, Gordon, R.G., 1998. Current plate motions across the Red Sea. Geophys. J. Int. 135, 313–328.

Coşkun, B., Coşkun, B., 2000. The Dead Sea Fault and related subsurface structures, Gaziantep Basin, southeast Turkey. Geol. Mag. 137, 175–192.

DeMets, C., Gordon, R.G., Argus, D.F., Stein, S., 1994. Effect of recent revisions to the geomagnetic time scale on estimates of current plate motions. Geophys. Res. Lett. 21, 2191–2194.

Dewey, J.F., Hempton, M.R., Kidd, W.S.F., Şaroğlu, F., Şengör, A.M.C., 1986. Shortening of continental lithosphere: the neotectonics of Eastern Anatolia—a young collision zone. In: Coward, M.P., Ries, A.C. (Eds.), Collision Tectonics, Spec. Publ.-Geol. Soc. London 19, pp. 3–36.

Domas, Y., 1994. The Late Cenozoic of the Al Ghab Rift, NW Syria. Sb. Geol. Věd, Antropozoikum 21, 57–73.

Dodonov, A.E., Deviatkin, E.V., Ranov, V.A., Khatib, K., Nseir, H., 1993. The Latamne Formation in the Orontes river valley. In: Sanlaville, P., Besançon, J., Copeland, L., Muhesen, S. (Eds.), Le Paléolithique de la vallée Moyenne de l'Oronte (Syrie): Peuplement et Environnement, Brit. Archaeol. Rev., Int. Ser. 587, pp. 189–194.

Dubertret, L., Vautrin, H., 1938. Sur l'existence du Pontien lacustre en Syrie et sur sa signification tectonique. C. r. Hebd. Séances Acad. Sci. 206, 69–71.

Ellembum, R., Marco, S., Agnon, A., Rockwell, T., Boas, A., 1998. Crusader castle torn apart by earthquake at dawn, 20 May 1202. Geology 26, 303–306.

Eyal, M., Eyal, Y., Bartov, Y., Steinitz, G., 1981. The tectonic development of the western margins of the Gulf of Elat (Aqaba) rift. Tectonophysics 80, 39–66.

Freund, R., Garfunkel, Z., Zak, I., Goldberg, M., Weissbrod, T., Derin, B., 1970. The shear along the Dead Sea rift. Philos. Trans. R. Soc. Lond. Ser. A: Math. Phys. Sci. 267, 107–130.

Garfunkel, Z., 1981. Internal structure of the Dead Sea leaky transform (rift) in relation to plate kinematics. Tectonophysics 80, 81–108.

Ginat, H., Enzel, Y., Avni, Y., 1998. Translocated Plio-Pleistocene drainage systems along the Arava Fault of the Dead Sea Transform. Tectonophysics 284, 151–160.

Girdler, R.W., 1990. The Dead Sea transform fault system. Tectonophysics 180, 1–13.

Gomez, F., Meghraoui, M., Darkal, A.N., Sbeinati, R., Darawcheh, R., Tabet, C., Khawlie, M., Charabe, M., Khair, K., Barazangi, M., 2001a. Coseismic displacements along the Serghaya Fault: an active branch of the Dead Sea fault system in Syria and Lebanon. J. Geol. Soc. (Lond.) 158, 405–408.

Gomez, F., Meghraoui, M., Darkal, A.N., Hijazi, F., Mouty, M., Souleiman, Y., Sbeinati, R., Darawcheh, R., Al-Ghazzi, R., Barazangi, M., 2001b. Holocene paleoseismic activity of the Serghaya branch of the Dead Sea fault system in Syria and Lebanon. Eos., Trans. AGU, Fall Meeting Suppl., Abstract S52C-0649, 929.Griffiths, H.M., Clark, R.A., Thorp, K.M., Spencer, S., 2000. Strain accommodation at the lateral margin of an active transpressive zone; geological and seismological evidence from the Lebanese restraining bend. J. Geol. Soc. (Lond.) 157, 289–302.

Hancock, P.L., Atiya, M.S., 1979. Tectonic significance of meso-fracture systems associated with the Lebanese segment of the Dead Sea transform fault. J. Struct. Geol. 1, 143–153.

Jackson, J.A., McKenzie, D.P., 1988. The relationship between plate motions and seismic moment tensors, and the rates of active deformation in the Mediterranean and Middle East. Geophys. J. 93, 45–73.

Karig, D.E., Kozlu, H., 1990. Late Palaeogene–Neogene evolution of the triple junction near Maraş, south-central Turkey. J. Geol. Soc. (Lond.) 147, 1023–1034.

Kempler, D., Garfunkel, Z., 1994. Structures and kinematics in the northeastern Mediterranean: a study of an irregular plate boundary. Tectonophysics 234, 19–32.

Khair, K., Tsokas, G.N., Sawaf, T., 1997. Crustal structure of the northern Levant region. Multiple source Werner deconvolution estimates for Bouguer gravity anomalies. Geophys. J. Int. 126, 605–616.

Klinger, Y., Avouac, J.P., Abou Karaki, N., Dorbath, L., Bourles, D., Reyss, J.L., 2000. Slip rate on the Dead Sea transform fault in northern Arava Valley (Jordan). Geophys. J. Int. 142, 755–768.

Kozlov, V., Artemov, A., Kalis. A. 1963. Geological map of the Trablus (I-36-XVIII) and Homs (I-37-XIII) quadrangles, 1:200,000 scale, and accompanying explanatory guide. Vsesoj. Exportno-Import Objed. Technoexport, Moscow, and Ministry of Industry. Syrian Arab Republic, Damascus.

Lovelock, P.E.R., 1984. A review of the tectonics of the northern Middle East region. Geol. Mag. 121, 577–587.

Matar, A., Mascle, G., 1993. Cinematique de la Faille du Levant au nord de la Syrie: analyse microtectonique du Fosse d'Alghab. Geodin. Acta 6, 153–160.

McClusky, S., 2000. Global Positioning System constraints on plate kinematics and dynamics in the eastern Mediterranean and Caucasus. J. Geophys. Res. 105, 5695–5719.

McKenzie, D.P., 1976. The East Anatolian fault: a major structure in eastern Turkey. Earth Planet. Sci. Lett. 29, 189–193.

Meghraoui, M., 2002. Large earthquake sequences along main continental faults: paleoseismic and historical constraints of the faulting behaviour. First International Symposium of the Faculty of Mines, İstanbul Technical University, on Earth Sciences and Engineering, Abstract Vol. İstanbul Technical University Press, İstanbul, pp. 57.

Meghraoui, M., Gomez, F., Sbeinati, R., Van Der Woerd, J., Mouty, M., Hijazi, F., Darkal, A.N., Darawcheh, R., Radwan, Y., Al-Najjar, H., Layous, I., Al-Ghazzi, R., Barazangi, M., 2001. Late Holocene paleoseismic timing and slip history along the Missyaf segment of the Dead Sea fault in Syria. Eos. Trans. AGU, Fall Meeting Suppl., Abstract S52C-0648, 929.

Meghraoui, M., Gomez, F., Sbeinati, R., Van Der Woerd, J., Mouty, M., Darkal, A.N., Radwan, Y., Layyous, I., Al-Najjar, H., Darawcheh, R., Hijazi, F., Al-Ghazzi, R., Barazangi, M., 2003. Evidence for 830 years of seismic quiescence from palaeoseismology, archaeoseismology and historical seismicity along the Dead Sea fault in Syria. Earth Planet. Sci. Lett. 210, 35–52.

Michard, A., Whitechurch, H., Ricou, L.E., Montigny, R., 1984. Tauric subduction (Malatya-Elazığ provinces) and its bearing on tectonics of the Tethyan realm in Turkey. In: Dixon, J.E., Robertson, A.H.F. (Eds.), The Geological Evolution of the eastern Mediterranean, Spec. Publ.-Geol. Soc. London vol. 17, pp. 362–373.

Mouty, M., Delaloye, M., Fontignie, D., Piskin, O., Wagner, J.-J., 1992. The volcanic activity in Syria and Lebanon between Jurassic and Actual. Schweiz. Mineral. Petrogr. Mitt. 72, 91–105.

Muehlberger, W.B., Gordon, M.B., 1987. Observations on the complexity of the East Anatolian fault, Turkey. J. Struct. Geol. 9, 899–903.

Perinçek, D., Çemen, I., 1990. The structural relationship between the East Anatolian and Dead Sea fault zones in southeastern Turkey. Tectonophysics 172, 331–340.

Perinçek, D., Kozlu, H., 1983. Stratigraphy and structural relations of the units if the Afşin-Elbistan-Doğanşehir region (eastern Taurus). In: Tekeli, O., Göncüoğlu, M.C. (Eds.), Geology of the Taurus Belt. Proceedings of the 1983 Ankara Symposium. General Directorate of Mineral Research and Exploration, Ankara, pp. 181–198.

Ponikarov, V.P., Kazmin, V.G., Mikhailov, I.A., Razvaliayev, A.V., Krasheninnikov, V.A., Kozlov, V.V., Soulidi-Kondratiyev, E.D., Faradzhev, V.A., 1966. The geological map of Syria, scale 1:1,000,000: explanatory notes. Vsesoj. Exportno-Import Objed. Technoexport, Moscow, and Ministry of Industry, Syrian Arab Republic, Damascus.

Ponikarov, V.P., Kazmin, V.G., Mikhailov, I.A., Razvaliayev, A.V., Krasheninnikov, V.A., Kozlov, V.V., Soulidi-Kondratiyev, E.D., Mikhailov, K.Y., Kulakov, V.A., Faradzhev, V.A., Mirzayev, K.M., 1967. The Geology of Syria: explanatory notes on the geological map of Syria, scale 1:500,000. Part I: Stratigraphy, Igneous Rocks, and Tectonics. Vsesoj. Exportno-Import Objed. Technoexport, Moscow, and Ministry of Industry, Syrian Arab Republic, Damascus.

Quennell, A.M., 1984. The Western Arabia rift system. In: Dixon, J.E., Robertson, A.H.F. (Eds.), The Geological Evolution of the

eastern Mediterranean, Spec. Publ.-Geol. Soc. London vol. 17, pp. 375–402.

Rojay, B., Heimann, A., Toprak, V., 2001. Neotectonic and volcanic characteristics of the Karasu fault zone (Anatolia, Turkey): the transition zone between the Dead Sea transform and the East Anatolian fault zone. Geodin. Acta 14, 197–212.

Şaroğlu, F., Emre, Ö., Kuşçu, İ., 1992. The East Anatolian fault zone of Turkey. Annales Tectonicae 6, 99–125.

Shatsky, V.N., Kazmin, V.G., Kulakov, V.V., 1963. Geological map of the Al-Latheqieh (I-36-XXIV) and Hama (I-37-XIX) quadrangles, 1:200,000 scale, and accompanying explanatory guide, 106 pp. Vsesoj. Exportno-Import Objed. Technoexport, Moscow, and Ministry of Industry, Syrian Arab Republic, Damascus.

Steinitz, G., Bartov, Y., Eyal, M., Eyal, Y., 1981. K–Ar age determination of Tertiary magmatism along the western margin of the Gulf of Elat. Geol. Surv. Israel Curr. Res. 1980, 27–29.

Ten Brink, U.S., Rybakov, M., Al-Zoubi, A.S., Hassouneh, M., Frieslander, U., Batayneh, A.T., Goldschmidt, V., Daoud, M.N., Rotstein, Y., Hall, J.K., 1999. Anatomy of the Dead Sea Transform; does it reflect continuous changes in plate motion? Geology 27, 887–890.

Terlemez, H.C.İ., Şentürk, K., Ateş, S., Oral, A., 1997. Geological Map of the Gaziantep-K24 Quadrangle, 1:100,000 scale, and Accompanying 18 page Explanatory Booklet. General Directorate of Mineral Research and Exploration, Ankara.

Tolun, N., Erentöz, C., 1962. Hatay Sheet of the Geological Map of Turkey, 1:500,000 scale. General Directorate of Mineral Research and Exploration, Ankara.

Tolun, N., Pamir, H.N., 1975. Explanatory Booklet Accompanying the Hatay sheet of the Geological Map of Turkey, 1:500,000 scale. General Directorate of Mineral Research and Exploration, Ankara. 99 pp.

Trifonov, V.G., Tribukhin, V.M., Adzhamyan, Z., Dshallad, S., El-Khair, Y., Ayed, K., 1991. Levant fault zone in northwest Syria. Geotectonics 25, 145–154.

Vidal, N., Alvarez-Marron, J., Klaeschen, D., 2000. Internal configuration of the Levantine Basin from seismic reflection data (eastern Mediterranean). Earth Planet. Sci. Lett. 180, 77–89.

Walley, C.D., 1988. A braided strike-slip model for the northern continuation of the Dead Sea fault and its implications for Levantine tectonics. Tectonophysics 145, 63–72.

Walley, C.D., 1998. Some outstanding issues in the geology of Lebanon and their importance in the tectonic evolution of the Levantine region. Tectonophysics 298, 37–62.

Westaway, R., 1990. Present-day kinematics of the plate boundary zone between Africa and Europe, from the Azores to the Aegean. Earth Planet. Sci. Lett. 96, 393–406.

Westaway, R., 1994. Present-day kinematics of the Middle East and eastern Mediterranean. J. Geophys. Res. 99, 12071–12090.

Westaway, R., 1995. Deformation around stepovers in strike-slip fault zones. J. Struct. Geol. 17, 831–847.

Westaway, R., 1999. Comment on "A new intracontinental transcurrent structure: the Central Anatolian Fault Zone, Turkey, by A. Koçyiğit and A. Beyhan". Tectonophysics 314, 469–479.

Westaway, R., 2002a. Discussion of "New sedimentological and structural data from the Ecemiş Fault Zone, southern Turkey: implications for its timing and offset and the Cenozoic tectonic escape of Anatolia" by N. Jaffey and A. H.F. Robertson. J. Geol. Soc. (Lond.) 159, 111–113.

Westaway, R., 2002b. The Quaternary evolution of the Gulf of Corinth, central Greece: coupling between surface processes and flow in the lower continental crust. Tectonophysics 348, 269–318.

Westaway, R., 2002c. Geomorphological consequences of weak lower continental crust, and its significance for studies of uplift, landscape evolution, and the interpretation of river terrace sequences. Neth. J. Geosci. 81, 283–304.

Westaway, R., 2002d. Long-term river terrace sequences: evidence for global increases in surface uplift rates in the Late Pliocene and early Middle Pleistocene caused by flow in the lower continental crust induced by surface processes. Neth. J. Geosci. 81, 305–328.

Westaway, R., Arger, J., 1996. The Gölbaşı basin, southeastern Turkey: a complex discontinuity in a major strike-slip fault zone. J. Geol. Soc. (Lond.) 153, 729–743.

Westaway, R., Arger, J., 2001. Kinematics of the Malatya–Ovacık fault zone. Geodin. Acta 14, 103–131.

Westaway, R., Pringle, M., Yurtmen, S., Demir, T., Bridgland, D., Rowbotham, G., Maddy, D., 2003. Pliocene and Quaternary surface uplift of western Turkey revealed by long-term river terrace sequences. Curr. Sci. 84, 1090–1101.

Yazgan, E., 1983. Geodynamic Evolution of the Eastern Taurus region. In: Tekeli, O., Göncüoğlu, M.C. (Eds.), Geology of the Taurus Belt. Proceedings of the 1983 Ankara Symposium. General Directorate of Mineral Research and Exploration, Ankara, pp. 199–208.

Yurtmen, S., Westaway, R., 2001. Intraplate alkaline volcanism to the north of İskenderun Gulf. Field Excursion Guide Book, Fourth International Turkish Geology Symposium. Çukurova University, Adana, Turkey. 28 pp.

Yurtmen, S., Westaway, R., 2001. Neogene to Quaternary volcanism and strike-slip faulting in the Gaziantep Plateau, southeastern Turkey. Fourth International Turkish Geology Symposium, September 2001, abstract volume. Çukurova University, Adana, Turkey, pp. 184.

Yurtmen, S., Rowbotham, G., İşler, F., Floyd, P., 2000. Petrogenesis of Quaternary alkali volcanics, Ceyhan–Turkey. In: Bozkurt, E., Winchester, J.A., Piper, J.D.A. (Eds.), Tectonics and Magmatism of Turkey and the Surrounding Area, Spec. Publ.-Geol. Soc. London vol. 173, pp. 489–512.

Yurtmen, S., Guillou, H., Westaway, R., Rowbotham, G., Tatar, O., 2002. Rate of strike-slip motion on the Amanos Fault (Karasu Valley, southern Turkey) constrained by K–Ar dating and geochemical analysis of Quaternary basalts. Tectonophysics 344, 207–246.

Zhang Hongwei, 1998. Late Pleistocene and Holocene slip rate of the northern Wadi Araba Fault, Dead Sea Transform, Jordan. Unpublished MS thesis, University of Missouri Kansas City, Kansas City, Missouri, USA, 128 pp.